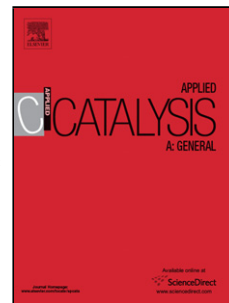


Journal Pre-proof

Silica/titania composite-supported NiCo catalysts with combined catalytic effects for phenol hydrogenation under fast and mild conditions

Yucheng Li (Methodology) (Investigation), Jing Liu (Formal analysis) (Writing - original draft), Jing He (Validation), Luying Wang (Writing - review and editing), Jiandu Lei (Supervision)



PII: S0926-860X(20)30002-8
DOI: <https://doi.org/10.1016/j.apcata.2020.117409>
Reference: APCATA 117409
To appear in: *Applied Catalysis A, General*
Received Date: 19 August 2019
Revised Date: 31 December 2019
Accepted Date: 2 January 2020

Please cite this article as: Li Y, Liu J, He J, Wang L, Lei J, Silica/titania composite-supported NiCo catalysts with combined catalytic effects for phenol hydrogenation under fast and mild conditions, *Applied Catalysis A, General* (2020), doi: <https://doi.org/10.1016/j.apcata.2020.117409>

This is a PDF file of an article that has undergone enhancements after acceptance, such as the addition of a cover page and metadata, and formatting for readability, but it is not yet the definitive version of record. This version will undergo additional copyediting, typesetting and review before it is published in its final form, but we are providing this version to give early visibility of the article. Please note that, during the production process, errors may be discovered which could affect the content, and all legal disclaimers that apply to the journal pertain.

© 2019 Published by Elsevier.

**Silica/titania composite-supported NiCo catalysts with combined catalytic effects
for phenol hydrogenation under fast and mild conditions**

Yucheng Li , Jing Liu * liujing@bjfu.edu.cn, Jing He , Luying Wang , Jiandu Lei *

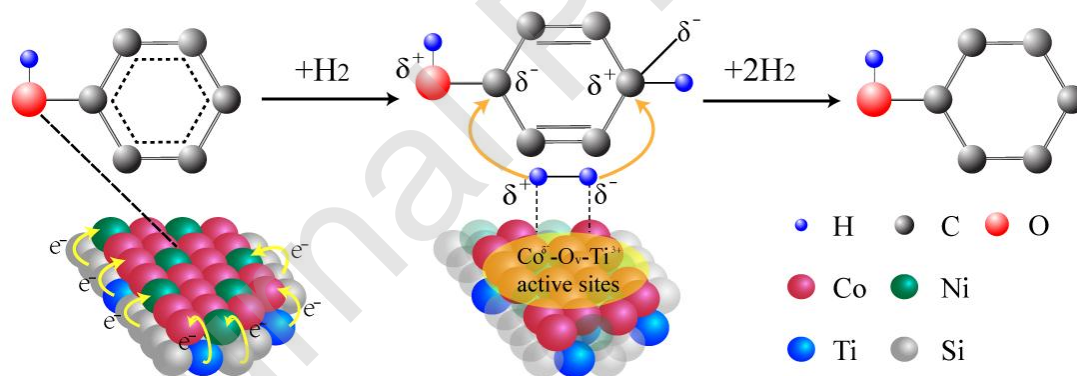
ljd2012@bjfu.edu.cn

Beijing Key Laboratory of Lignocellulosic Chemistry, Beijing Forestry University,

Beijing 100083, P. R. China

* Corresponding author. Tel: +86 10 6233 7251

Graphical abstract



Highlights

- Hydrogenation phenol to cyclohexanol using NiCo/Si-Ti catalyst was completed within 1 h under mild reaction conditions (1 MPa H_2 and $100^{\circ}C$).

- NiCo/Si-1.0Ti (Si:Ti ratio of 8.5:1) catalyst was more efficiently (conversion 98.2% and selectivity >99%) than NiCo/Si and other Ti-doped catalysts.
- Ti-promoter induces the formation of the $\text{Co}^{\delta-}-\text{O}_V-\text{Ti}^{3+}$ active sites and enhances the hydrogenation activity.
- The NiCo/Si-1.0Ti catalysts showed a good performance at reducing the unstable oxygenated compounds in the real bio-oil.
- The kinetics, pathway and catalytic mechanism of the hydrogenation of phenol are examined.

Abstract

The effect of titanium as a promoter for the nickel-cobalt/silica-titania (NiCo/Si-Ti) catalyst in the hydrogenation of phenol was comparatively studied. In the phenol hydrogenation under mild reaction conditions (1 MPa H_2 pressure and 100°C), the Ti-promoter induces the formation of the $\text{Co}^{\delta-}-\text{O}_V-\text{Ti}^{3+}$ active sites and enhances the hydrogenation activity of the NiCo/Si catalyst to convert phenol to cyclohexanol. The catalytic hydrogenation with the optimal composition of the NiCo/Si-1.0Ti (Si:Ti ratio of 8.5:1) catalyst was completed within 1 h (conversion 98.2% and selectivity >99%), which was more efficiently than that with other Ti-doped catalysts and NiCo/Si as baseline, indicating a strong positive synergistic effect between the metal (Ni-Co) and support (Ti-Si) components of the catalyst in this reaction. Additionally, the kinetics, pathway and catalytic mechanism of the hydrogenation of phenol are also examined. Furthermore, the NiCo/Si-1.0Ti catalysts also showed a good performance at reducing the unstable oxygenated compounds in the bio-oil.

Keywords: Silica/titania composite; NiCo catalyst; Phenol hydrogenation;

Cyclohexanol; Mild condition

1. Introduction

Recognized as an environmentally-friendly alternative resource, biomass has been increasingly drawing worldwide attention. As the most abundant component of biomass [1], many efforts have been made to efficiently use lignocellulosic materials by fast pyrolysis, gasification, combustion and liquefaction. Among these processes, fast pyrolysis is considered as one of the most promising approaches for the efficient conversion of biomass to bio-oil with high yields (up to 60 wt%) through thermal decomposition and depolymerization of macromolecules [2]. Bio-oil can be produced by pyrolysis, liquefaction, transesterification and other processes. It is mainly composed of oxygenated aromatic compounds, such as phenols, furans, ketones, aldehydes, alcohol, ether, acids and esters [3], with a content of phenolic aromatic compounds over 55% [4]. Phenol, the most representative of the phenolic compounds, as a common byproduct of the petrochemical industry, can cause considerable damage to the environment [5].

The hydrogenation of phenol is an important process in the chemical synthesis of raw materials (e.g. cyclohexanone and cyclohexanol) for the production of various products, such as nylon, fuel, pharmaceuticals, plasticizers, surfactants, solvents, *etc.*, which play a critical role in economic and societal development [6]. In fact, besides its much lower toxicity than phenol and cyclohexanone [7], cyclohexanol is an

important intermediate for the synthesis of Nylon-6 and the component of ketone-alcohol (KA) oil in petroleum industry [8, 9], Additionally, cyclohexanol is also an effective oxygenate additive for the enhancement of the multi-component diesel fuel used to improve emissions [10]. Thus, the selective hydrogenation of phenol appears to be an effective alternative route to produce cyclohexanol, where a highly-efficient catalyst is crucial for industrial applications [11].

According to the literature, commonly used catalysts for the hydrogenation of phenol are transition metals (like Ni, Co, and Ce) [12-14], and noble metals (such as Pt, Pd, Ru, *etc.*) [15-18], loaded into oxyphilic supports, such as Al₂O₃, SiO₂, and ZrO₂ [19-22]. Undoubtedly, noble metal catalysts are expensive and sulfurated catalysts [3] cause environmental problems, which limit their application on an industrial scale. Due to their low cost and abundance, the Ni-based bimetallic and trimetallic alloy catalysts have been synthesized and used in the hydrogenation of phenol [23, 24] which is usually chosen as a model bio-oils compound [25, 26]. Aiqin Li *et al.* [11] prepared a bimetallic metal-organic framework (MOF)-derived Co-Ni@NC catalyst for the selective hydrogenation of phenol and the sole product was cyclohexanol. They found that the catalyst with the optimal composition (1Co-1Ni@NC-600) was able to completely catalyze the hydrogenation of phenol to >99.9% cyclohexanol with an activity up to 2.8 and 4.3-fold higher than that of the catalysts Co@NC and Ni@NC, respectively. However, the complicated MOF-templated synthesis (more than 72 h) and high calcination temperature (reached 600°C) of the catalyst may limit its application in industry. Recent studies have reported that Ni- and Co-based

catalysts ($\text{Ni}_x\text{Co}_y\text{@C/ZrO}_2$) supported by a Zr-based MOF have the best catalytic performance at the desired temperature of 200°C for 240 min, with a 96.33% conversion of phenol and a cyclohexanol selectivity of 91.14% [27]. Yuzhen Shi et al. [28] obtained a total mole yield of 80% and a selectivity of 80% using 15 wt% of the Ni–Co/ γ - Al_2O_3 catalyst. Therefore, high activity (>99%) non-noble metal catalysts at faster reaction rate (<60 min) and under milder reaction condition (<100°C) are coveted in phenol hydrogenation.

In this study, Ti-Si-supported Ni and Co metal catalysts were synthesized and used for phenol hydrogenation to prepare cyclohexanol. Titanium oxide was used to enhance the active sites on the catalyst. Besides the preparation of the catalysts, we focused on its characterization and evaluation of its performance in the conversion, selectivity and kinetics during phenol hydrogenation under mild conditions. In addition, the pathway of phenol hydrogenation and metal–support interaction were also examined. Moreover, the selected catalyst (NiCo/Si-1.0Ti) was experimentally used for the hydrogenation of real bio-oil.

2. Experimental and methods

2.1 Material

Ammonia (14%), Cetyltrimethylammonium, Tetrabutyl titanate (99%; Macklin Biochemical Co., Ltd., Shanghai, China), Ethyl orthosilicate (99%; Macklin Biochemical Co., Ltd.), $\text{Ni}(\text{NO}_3)_2$, $\text{Co}(\text{NO}_3)_2 \cdot 6\text{H}_2\text{O}$, Hexane (99%; Alfa-Aesar Chemicals, Tewksbury, MA, USA), n-Heptane (>99%; Aladdin Biochemical

Technology Co., Ltd.), n-Dodecane (99%; Macklin Biochemical Co., Ltd.) and Phenol (AR, Xilong Scientific Co., Ltd.) are all commercially available and used without further purification. Bio-oil as feedstock in this work was produced by pyrolyzing walnut shell at 530 °C, which was provided by University of Science and Technology of China. The pyrolysis-condensation device and experimental details were described by Chu Wang et al [29].

2.2 Synthesis of catalysts

Templated synthesis. A solution of ammonia water (3.25 mL), cetyltrimethylammonium (CTACL, 16.58 g) and water (243 mL) was prepared by mixing and stirring at room temperature for 12 h. Subsequently, ethyl orthosilicate (TEOS) and butyl titanate (TBOT) were added dropwise to the above solution with agitation. The amount of Si and Ti precursor was varied in order to prepare four catalysts with different Si:Ti ratios of 8.5:1.0, 6.0:3.5, 3.5:6.0 and 1.0:8.5. The resulting samples were denoted as Si-1.0Ti, Si-3.5Ti, Si-6.0Ti and Si-8.5Ti, respectively. Then the obtained mixture was vacuum dried at 90°C for 3 h. After the gelatin formed, it was ground into a powder to obtain the titanium-silicon carrier.

Metal impregnation. Ni(NO₃)₂ (1 g), Co(NO₃)₂·6H₂O (1.5 g) and titanium-silicon carrier (1.5 g) prepared above were dispersed in 20 mL normal hexane reflux for 12 h at 70°C. After cooling, the resulting slurry was centrifuged in 3000 rpm for 5 min. The precipitate was dried in air at room temperature for 12 h, then dried at 60°C for 3 h under vacuum. Subsequently, the solid products were calcined at 450°C for 4.5 h with heating rate of 10°C min⁻¹. After cooling, the solid products were treated with a

sodium hydroxide solution (15% wt%) for 5 h at room temperature, to obtain the NiCo/Si-1.0Ti, NiCo/Si-3.5Ti, NiCo/Si-6.0Ti and NiCo/Si-8.5Ti catalysts. NiCo/Si catalyst was also prepared by using above method with no Ti. Ultimately, the catalysts were reduced under a flow of 50% v/v N₂/H₂ (50mL/min) at 300°C for 3 h. The typical synthetic method for the preparation of the NiCo/Si-Ti catalyst is schematically illustrated in Fig. 1.



Fig. 1 Schematic of synthesis of NiCo/Si-Ti catalysts and their hydrogenation performance of phenol.

2.3 Catalyst evaluation

2.3.1 Phenol hydrogenation

About 0.05 g of phenol and 0.1 mL n-tetradecane (as the internal standard substance) were dissolved in 10 mL of n-heptane and placed in a 50-mL stainless steel cylinder reactor, followed immediately by the addition of 0.1 g of fresh catalyst into the reactor. The reactor was charged with N₂ gas (99.999%) three times at 0.2 MPa to displace the air from the chamber, and then filled up three times with H₂ gas at 0.2 MPa to displace the N₂. After repeated charging and venting, the H₂ pressure was raised to 1 MPa and the reactor was placed on a heater with matched temperature controller to

maintain the reactor at 100°C with stirring at a speed of 300 rpm. After heating for 2 h, the reactor was removed from the heater and allowed to cool to room temperature with a fan. The products of the phenol hydrogenation reaction were analyzed by gas chromatography (GC) using the Agilent 7890B GC system (Agilent Technologies, Santa Clara, CA, USA), equipped with a flame ionization detector (FID), using a 330 mm × 0.32 mm × 0.25 μm Agilent HP-5 capillary column. The GC system was operated at 40°C for 4 minutes and increased to 260°C at a rate of 15°C/min. The results were calculated using the follow equations [10]:

$$\text{Phenol conversion} = \left(1 - \frac{\text{mol of Phenol after reaction}}{\text{mol of Phenol initial}}\right) \times 100\%$$

$$\text{Cyclohexanol selectivity} = \frac{\text{mol of Cyclohexanol}}{\text{mol of the amounts of products}} \times 100\%$$

2.3.2 Hydrogenation of real biofuel.

Hydrogenation of bio-oil was carried out in a 50-mL stainless steel cylinder reactor.

The prepared catalyst (0.5 g) and bio-oil (10 mL) were added into the reactor. The reactor was then subjected to the same in-reactor gas treatment described above.

Afterwards, the reactor was heated to the reaction temperature of 250°C with stirring at 300 rpm. Eventually, the reactor was quickly cooled to room temperature with a fan.

The liquid reaction products were separated from the catalysts by centrifugation and analyzed by Gas Chromatography-Mass Spectrometry (GC-MS) using the Agilent 7890A/5975C GC-MS system (Agilent Technologies), equipped with a BPX-70 capillary column. The GC-MS system was operated as described for the GC system above. Functional groups of raw bio-oil and hydrogenated bio-oil were characterized by nuclear magnetic resonance spectroscopy (NMR) using a Bruker AVIII 400 MHz

NMR (Bruker, Germany) as described in the literature [30].

2.4 Catalysts characterization

The phase composition and crystal structure of the catalysts were investigated by X-ray diffraction (XRD) analysis, performed on a Rigaku D/MAX-III A X-ray diffractometer (Rigaku Corp., Tokyo, Japan) operated at 3 kW and using Cu K α radiation. The scanning speed was at 2°/min in the scanning region of 10-90°. N₂ adsorption-desorption isotherms of the catalysts were recorded at 77K on a Micromeritics TriStar 3000 apparatus (Micromeritics Instrument Corp., Norcross, GA, USA). H₂ temperature-programmed desorption (H₂-TPD) analyses of the final catalyst were performed using a TP-5080 Multi-functional Automatic Adsorption Instrument (Tianjin Xianquan Company, Tianjin, China). First, 100 mg of the catalyst samples were pretreated for 20 min at 400°C, under a N₂ atmosphere. Then, the adsorption of H₂ was measured under a mixed flow of H₂ (30 mL/min) and N₂ (30 mL/min) at 400°C for 1 h and then slowly decreased from 400 to 20°C. Next, the H₂ weakly absorbed on the sample was removed by flushing with a N₂ stream (30 mL/min, 20°C, 15 min) and the strongly absorbed H₂ was detected by H₂-TPD method. The H₂ desorption curves were obtained under an N₂ stream of 30 mL/min at a temperature increasing linearly from 20, to 1,000°C at 10°C/min. The desorbed H₂ was monitored on-line using a GC system equipped with a thermal conductivity detector (TCD). The specific surface areas were determined by Brunauer-Emmett-Teller (BET) method and the pore size distribution and pore volume were calculated by the Barrett-Joyner-Halenda (BJH) method. The microscopic features such as the surface

topography and element distribution of the catalyst were examined by transmission electron microscope (TEM) on a JEM-1010 transmission electron microscope (JEOL Ltd., Tokyo, Japan), scanning electron microscope (SEM) on a SU8010 scanning electron microscope (JEOL Ltd.) equipped with an energy-dispersive X-ray spectrometer (EDS) accessory, and high-resolution transmission electron microscopy (HRTEM) on a JEM-2100F transmission electron microscopy (JEOL Ltd.) equipped with an EDS. The content and chemical states of the elemental constituents were analyzed by X-ray photoelectron spectroscopy (XPS) on an EscaLab 250Xi X-ray photoelectron spectrometer (Thermo Fisher Scientific, Waltham, MA, USA). FT-IR spectra in the region $500\text{-}4000\text{ cm}^{-1}$ were recorded using a Bruker VERTEX 70 FT-IR spectrophotometer (Bruker Optik GmbH, Ettlingen, Germany) with KBr pellets.

3. Results and discussion

3.1 Characterizations of the catalysts.

The SEM images showing the surface morphology of the Si-1.0Ti, NiCo/Si-1.0Ti and NiCo/Si-8.5Ti catalyst are displayed in Fig. 2(a)-(c), respectively, while Fig. 2(d)-(f) display the TEM images of the NiCo/Si, NiCo/Si-1.0Ti and NiCo/Si-8.5Ti catalysts. HRTEM images of NiCo/Si-1.0Ti and NiCo/Si-8.5Ti catalysts were showed in Fig. S1, and some micropore below 2 nm appeared in NiCo/Si-1.0Ti catalyst. These SEM and TEM images revealed the characteristic porous surface of all the catalysts examined. They show that the porosity decreased when Si:Ti ratio from 8.5:1 change to 1:8.5 (proved by BET results below). The highly uniform porous structure is great

beneficial to improve the catalytic performance. Additionally, the HRTEM-EDS (Fig. 2g) images show that all elements are evenly distributed with no formation of aggregates. The estimated Ti, Ni and Co content was 4.12, 13.68 and 22.12 wt%, respectively.

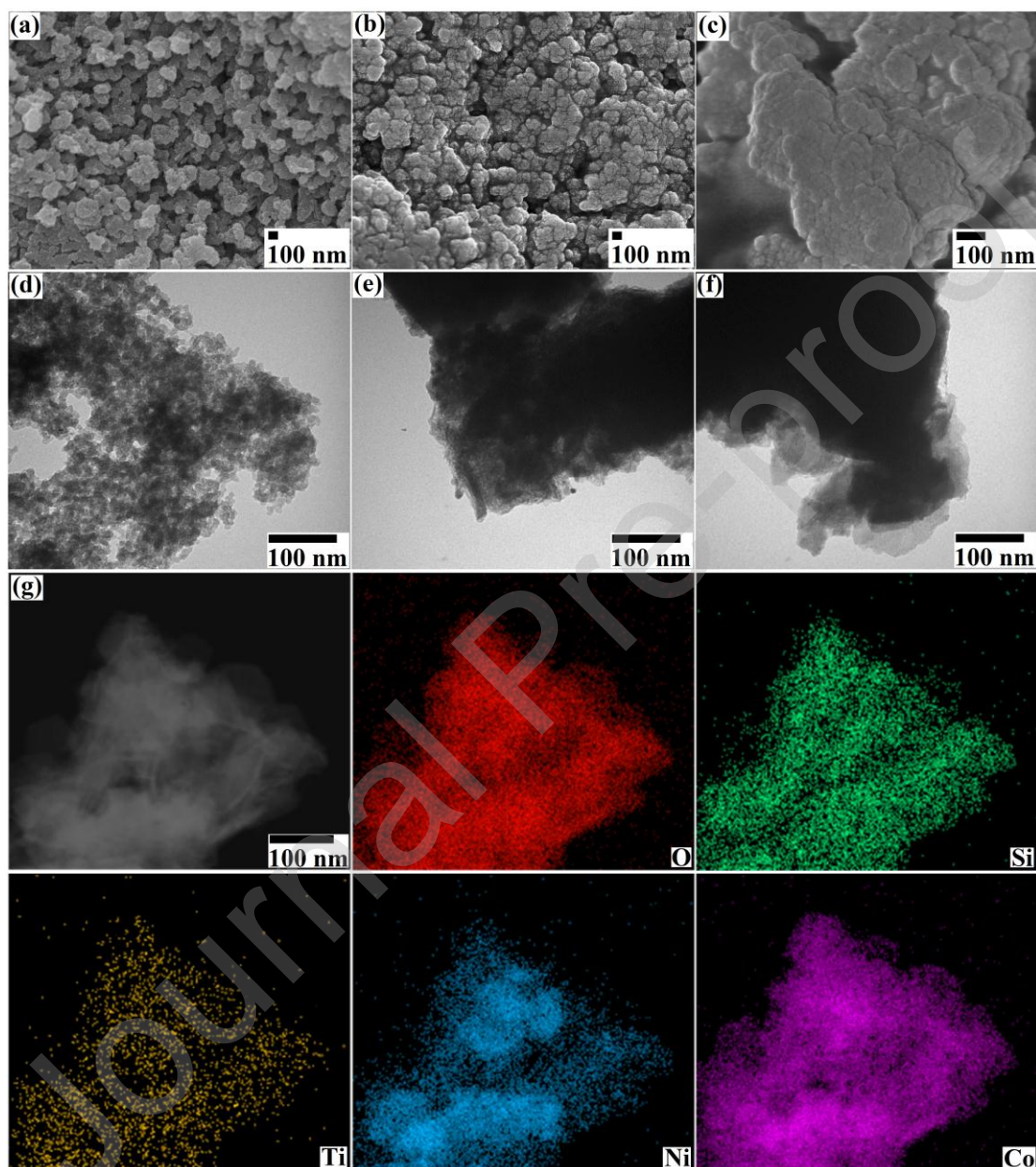


Fig. 2 SEM images of Si-1.0Ti (a), NiCo/Si-1.0Ti (b) and NiCo/Si-8.5Ti(c); TEM images of NiCo/Si (d), NiCo/Si-1.0Ti (e) and NiCo/Si-8.5Ti (f); HRTEM-EDS elemental mappings for NiCo/Si-1.0Ti (g).

The N₂ adsorption-desorption isotherms and pore size distribution curves of the catalysts are displayed in Fig. 3, and the details of their physical properties are shown in Table 1. All the samples displayed type IV N₂ adsorption-desorption isotherms, as can be seen in Fig. 3a, and showed an H4 hysteresis loop (according to the IUPAC classification), indicating its dominating mesoporous structure [31]. Also, the hysteresis loop becomes narrower with the addition of Ti, which indicates the decrease of the mesoporosity [32], leading to decrease of BJH pore volume (see Table 1). Additionally, as shown in Fig. 3b, the porosity decreased with the increase in the Ti content for Ti-doped catalysts. The data presented in Table 1 revealed that NiCo/Si-1.0Ti catalyst had the highest specific surface area (56.64 m²/g), BJH pore volume (0.12 cm³/g) and SF micropore volume (0.02 cm³/g) among all catalysts. However, the specific surface area and pore volume of the Ti-doped catalyst slightly decrease with increasing Ti content, which can be attributed to the blockage of the small pores of NiCo/Si-1.0Ti. Compared to the baseline NiCo/Si, there is an increase in surface area for all of the Ti-doped catalysts and an increase in pore diameter for higher Ti-doped catalysts (3.5Ti, 6.0Ti and 8.5Ti). Such an increase is probably because Ti-precursor decomposed leading to pore formation.

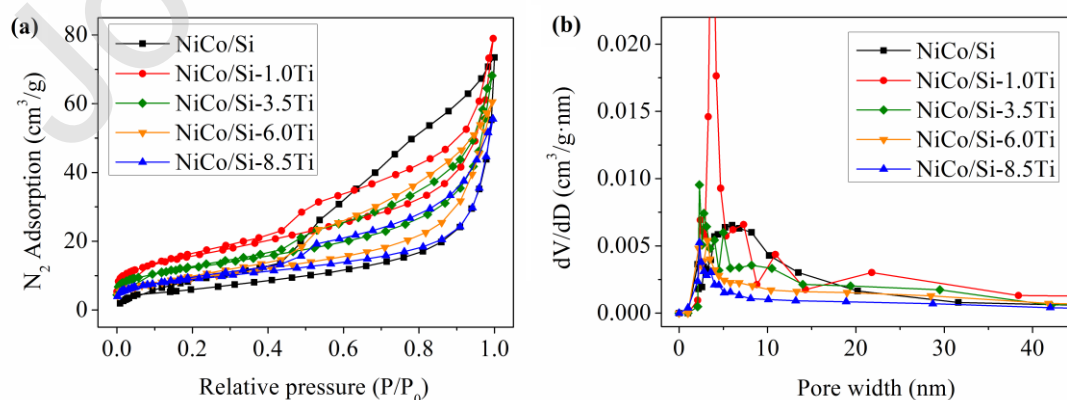


Fig. 3 The N₂ adsorption-desorption isotherms (a) and pore size distribution (b) of the NiCo/Si, NiCo/Si-1.0Ti, NiCo/Si-3.5Ti, NiCo/Si-6.0Ti and NiCo/Si-8.5Ti catalysts.

Table 1 Surface area, pore size and pore volume of catalysts.

Catalyst	BET surface area (m ² /g)	BJH pore diameter (nm)	BJH pore volume (cm ³ /g)	SF micropore volume (cm ³ /g)
NiCo/Si	29.83	11.65	0.12	0.01
NiCo/Si-1.0Ti	56.64	11.00	0.12	0.02
NiCo/Si-3.5Ti	44.15	11.98	0.10	0.02
NiCo/Si-6.0Ti	33.33	12.81	0.09	0.01
NiCo/Si-8.5Ti	32.06	14.47	0.08	0.01

The XRD patterns of the NiCo/Si, NiCo/Si-1.0Ti, NiCo/Si-3.5Ti, NiCo/Si-6.0Ti and NiCo/Si-8.5Ti catalysts are shown in Fig. 4(a). The XRD pattern of all catalysts clearly reveal the oxide phases of cobalt (Co₃O₄ 2 θ at 19.08, 32.03, and 36.80°) [9, 33], and nickel (NiO 2 θ at 37.70, 43.13 and 62.88°) [34, 35]. The weak peak at 2 θ = 51.44° assigned to metallic Ni (JCPDS No. 04-0850) [36] or metallic Co (JCPDS No. 15-0806) [37], confirming the presence of slight metallic Ni and/or Co in the all catalysts. In fact, the crystalline phases of metallic Ni and Co have similar diffraction patterns, making their identification difficult. The SiO₂ exhibits amorphous XRD patterns with some small peaks at 2 θ = 23-25° (ICSD No. 47219) [38]. No crystalline peaks corresponding to TiO₂ are observed in the spectra of the all catalysts. We considered the lower concentration of TiO₂ was so uniformly dispersed on the surface of catalysts that it is not detectable by XRD analysis. However, for NiCo/Si-1.0Ti, the

diffraction peak ($2\theta=36.80^\circ$) of Co_3O_4 shifts toward high angles ($2\theta=37.21^\circ$), indicating the probable formation of Co-Ti alloy [11, 39]. It is strange that NiCo/Si-3.5Ti, NiCo/Si-6.0Ti and NiCo/Si-8.5Ti catalysts were hardly observed the slight variation in this peak position. We consider that Co-Ti alloy appeared in NiCo/Si-1.0Ti is the most significant. This indicates the occurrence of structural and physicochemical changes in the hydrogenation catalyst, which may result in differences in the catalytic performance.

As shown in Fig. 4(b), the H_2 -TPD spectra obtained for NiCo/Si, NiCo/Si-1.0Ti, NiCo/Si-3.5Ti, NiCo/Si-6.0Ti and NiCo/Si-8.5Ti catalysts displayed a broad profile at low temperature (around 130°C). These spectra show that Ti-doped catalysts markedly enhance H_2 uptake compared with the NiCo/Si catalyst, and the peak intensity of the Ti-doped catalysts are all higher than that of the NiCo/Si catalyst. It can be also observed that H_2 desorption peak at 136°C for NiCo/Si-1.0Ti catalysts slightly shifts to lower temperature (126°C for NiCo/Si-8.5Ti catalysts) with increasing Ti content, suggesting that more Ti content leads weaker interaction between active metals and adsorbed H_2 . It is important to note that there is a high-temperature desorption peak (around 530°C) only in the NiCo/Si-1.0Ti, NiCo/Si-3.5Ti, and NiCo/Si-6.0Ti catalysts, indicating that H_2 strongly chemisorbed on the surface of these catalysts. But NiCo/Si-8.5Ti catalyst showed no high-temperature desorption peak below 600°C . All in all, NiCo/Si-1.0Ti catalyst displayed the most intense H_2 desorption peak in the H_2 -TPD profiles, suggesting that it had the most abundant dissociated active H, and the strongest interaction between

activating centers and adsorbed H₂ [31].

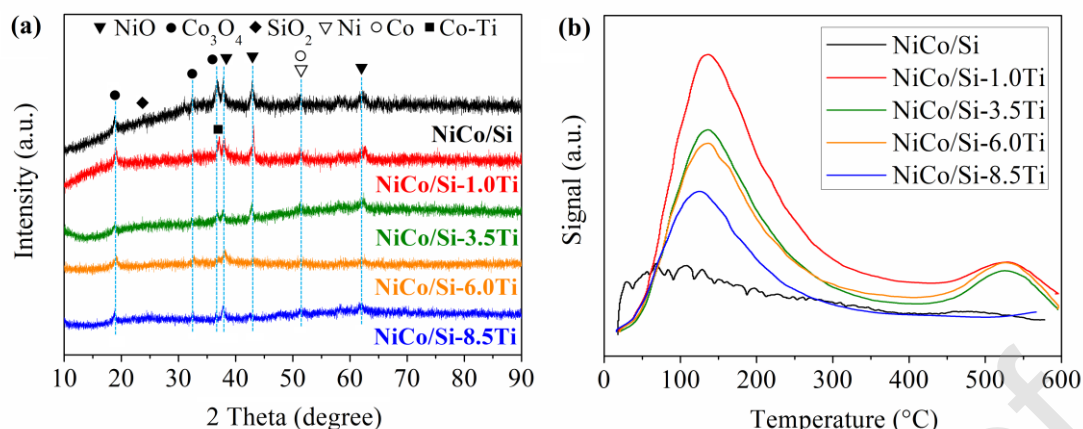


Fig. 4 XRD patterns (a) and H₂-TPD profiles (b) of the NiCo/Si, NiCo/Si-1.0Ti, NiCo/Si-3.5Ti, NiCo/Si-6.0Ti and NiCo/Si-8.5Ti catalysts.

In the FT-IR spectra of all samples (Fig. 5), the broad peaks at around 3434 cm⁻¹ were assigned to the stretching vibrations of Si-OH present in the support and the O-H associated to free water and structural water contained in the sample [40]. A sharp peak observed at 1633 cm⁻¹ was assigned to the O-H bending vibration of the adsorbed water molecules [41]. The IR absorption at 984 cm⁻¹ was ascribed to the vibration of Si-OH [42-44]. As shown in Fig. 5, there is no obvious difference between the spectra of the fresh NiCo/Si-1.0Ti and used NiCo/Si-1.0Ti, with the expected new characteristic peaks at around 2920 cm⁻¹ and 1148-1123 cm⁻¹, attributed to the stretching vibrations of C-H and the C-O-C groups [45], resulting from the carbonaceous accumulation around the used catalyst. It can also be seen that the IR spectra of NiCo/Si showed a strong vibration absorption band at 1015 cm⁻¹, which was assigned to the vibration of Si-O-Si bonds [46-48]. However, for NiCo/Si-1.0Ti, the vibration band was shifted to 1031 cm⁻¹, indicating the effective

coordination interaction between Si and Ni, which was further confirmed by the XPS analysis, which will be discussed later. It is strange that no Si–O–Si vibration peak was present in NiCo/Si-8.5Ti, we speculate that it is not detected by FT-IR spectroscopy due to its lower Si content. All samples had peaks below 600 cm^{-1} , which were ascribed to the symmetric stretching vibration of metal-oxygen groups [49], and the band at about 562 cm^{-1} was assigned to Ni-O [50]. The characteristic peak at around 462 cm^{-1} was ascribed to the stretching vibration absorption of Si-O, Ti-O bonds [51-53] or Ni-O and Co-O bonds [54]. Importantly, although the Ti content in NiCo/Si-1.0Ti was lower than that in NiCo/Si-8.5Ti, the intensity of the metal-oxygen groups was higher. This may lead to stronger interaction between the activating centers and adsorbed H_2 (proved by H_2 -TPD). In addition, the absorption peaks around 500 cm^{-1} were attributed to the stretching vibration of Ti-O-Ti [55, 56], indicating that TiO_2 was still remain in the spent catalysts. According to the relevant literature [57], the absorption bands at around 950 cm^{-1} corresponding to the Ti–O–Si bond was not detected in the spectrum, revealing that there was not obvious interaction between Ti and Si.

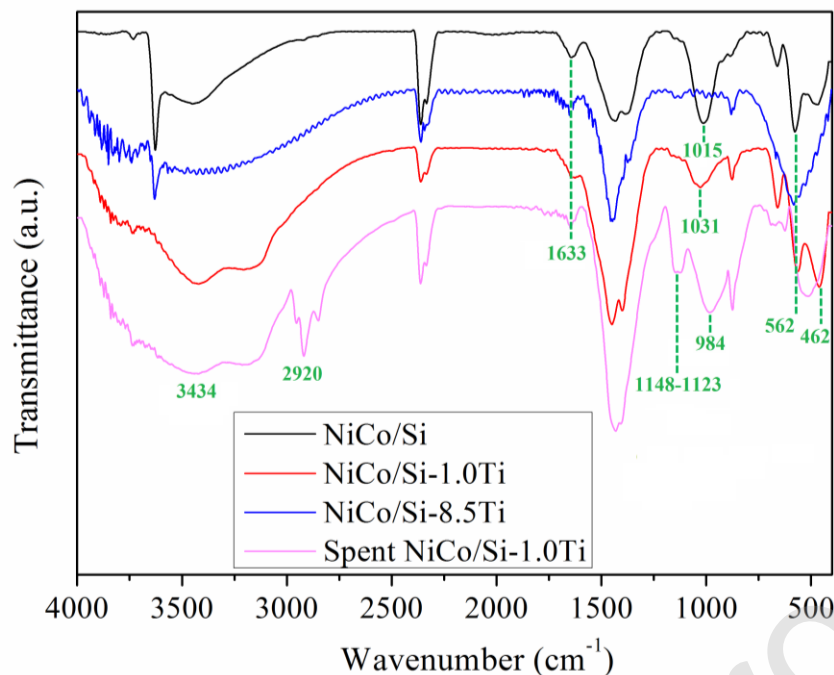


Fig. 5 FT-IR spectra of NiCo/Si, NiCo/Si-1.0Ti, NiCo/Si-8.5Ti and spent NiCo/Si-1.0Ti catalysts.

The wide scanning spectra (Fig. 6a) indicates that the NiCo/Si, NiCo/Si-1.0Ti and NiCo/Si-8.5Ti catalysts are mainly composed of Ni, Co, O, Si and/or Ti elements. The high-resolution XPS spectra of Ni 2p, Co 2p, O 1s, Si 2p and Ti 2p are shown in Fig. 6(b-f). The analysis of the Ni 2p spectra (Fig. 6b) indicates out that Ni is mainly in the oxidized state [58]. Four characteristic peaks, i.e. Ni 2p_{3/2} main peak and its satellite peak at ca. 855 and 861 eV, respectively, as well as Ni 2p_{1/2} main peak and its satellite peak at ca. 873 and 879 eV, respectively, are in good agreement with Ni²⁺ [59, 60]. The peak at the binding energy of 101.46 eV is assigned to Si 2p (Fig. 6c). Compared with the NiCo/Si catalyst, the characteristic peaks attributed to the Ni 2p_{3/2} and Ni 2p_{1/2} species in the NiCo/Si-1.0Ti sample were shifted to lower binding energy (-0.54 eV and -0.67 eV, respectively). As anticipated, a positive shift (+0.27 eV) of the peak ascribed to Si 2p in the NiCo/Si-1.0Ti sample was observed compared with that in

NiCo/Si. This is attributed to certain charge transfer from Si to the Ni atom. These results indicated that there must be stronger interaction between Ni and Si in NiCo/Si-1.0Ti than that in NiCo/Si. Thus, Ti doping in the NiCo/Si catalysts leads to change in the electron density and charge distribution of the atoms on the surface of the catalyst, which is beneficial for improving the activity of the catalyst.

The spectrum of O 1s (Fig. 6d) shows one peak at 530.85 eV for NiCo/Si. The asymmetrical O 1s region of NiCo/Si-1.0Ti and NiCo/Si-8.5Ti can be divided into two peaks at ca. 529 and 531 eV. The peaks at 529.34 and 529.06 eV are related to the TiO₂ lattice oxygen (Ti-O bond) for NiCo/Si-1.0Ti and NiCo/Si-8.5Ti, respectively, and those at 530.85 and 530.67 eV are attributed to adsorbed water or hydroxyl groups on the surface of catalysts [61], which was confirmed by the FT-IR spectroscopy results.

According to the data in Fig. 6e, the Ti 2p_{3/2} and Ti 2p_{1/2} binding energies were observed at ca. 457 eV and 463 eV for the two samples that were identified as TiO₂ [62, 63], and the binding energy of Ti 2p decreased with increasing Ti content.

Moreover, in Fig. 6f, the Co 2p_{3/2} peaks in the spectra of NiCo/Si-1.0Ti and NiCo/Si-8.5Ti are located at 780.07 and 779.79 eV, respectively, which exhibited slight downshifts compared to that of NiCo/Si (780.19 eV). These shifts to lower values can be indicative of the occurrence of metallic synergic effects [11], and the electron density gradually increases at the interface of the Co atoms and forms Co^{δ-} [64].

The strong metal–support interaction (SMSI) could explain this phenomenon [34].

The overflowing H₂ hydrogen from the surface of metallic Co diffuses onto the reducible TiO₂ surface to form partially reduced titania (TiO_{2-x}). The transfer of electron from TiO_{2-x} to the adjacent metal Co atoms causes electron enrichment at the interface of Co atoms. In the meantime, the strong Co–TiO_{2-x} electronic interaction can promote the formation of the oxygen vacancies of titania species (i.e., O_v–Ti³⁺ sites) near the perimeter of the metal–support interface and form the Co^{δ-}–O_v–Ti³⁺ interface sites, which play an important role as active sites for the catalytic hydrogenation of phenol [65-67]. Furthermore, the shapes of the Si 2p and Ni 2p spectra of NiCo/Si-1.0Ti and NiCo/Si-8.5Ti remained similar for different Ti loadings, and almost no electrons from the Si 2p and Ni 2p were transferred between NiCo/Si-1.0Ti and NiCo/Si-8.5Ti, indicating that Ti content does not affect the state of the Si and Ni species.

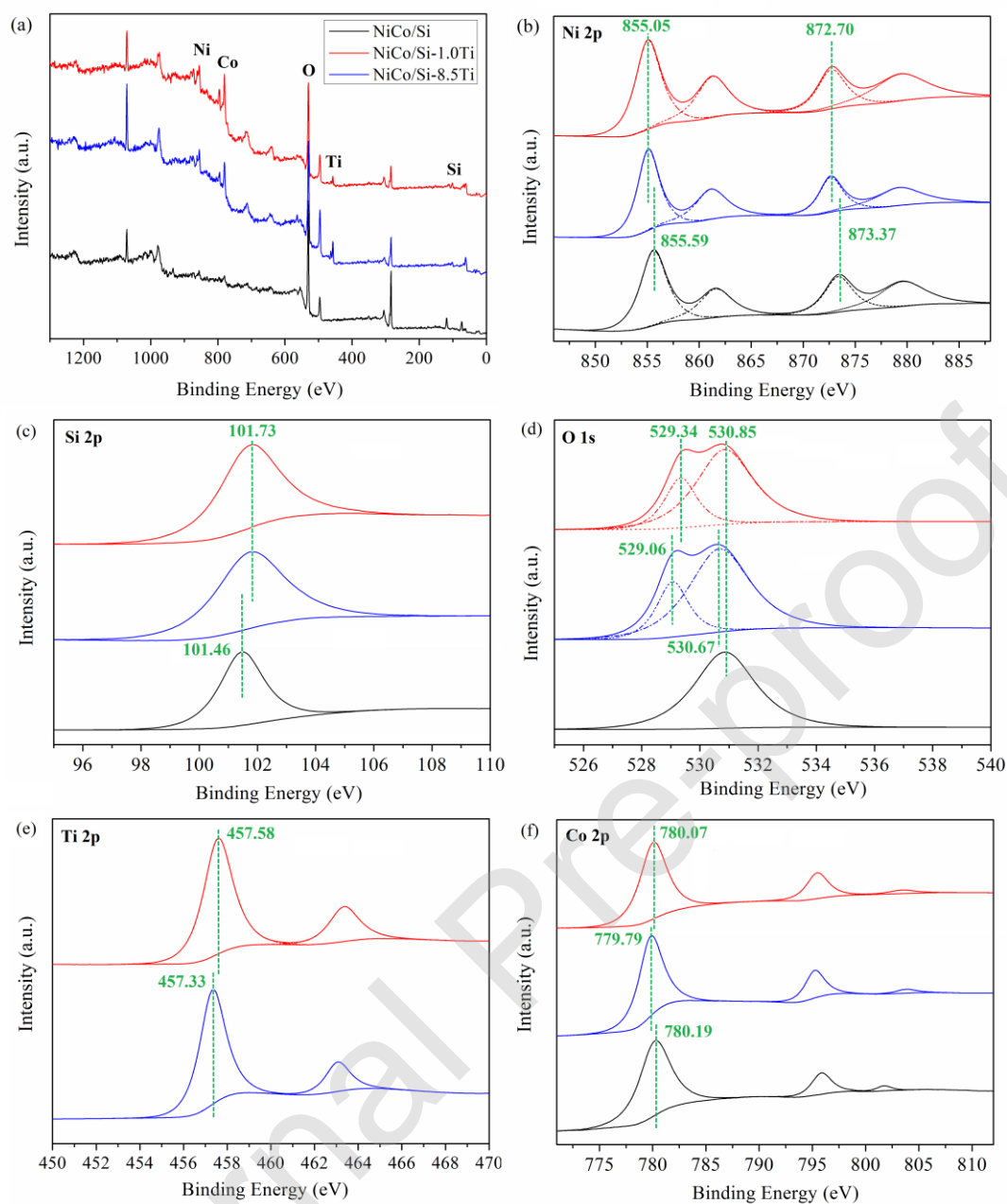


Fig. 6 XPS spectra of NiCo/Si, NiCo/Si-1.0Ti and NiCo/Si-8.5Ti.

3.2 Catalyst evaluation

In this work, the effect of different metal combinations and carrier types on the hydrogenation of phenol was studied in the presence of 0.1 g catalyst and 0.05 g phenol with 10 mL n-heptane at 100°C for 0.5 h. As shown in Table 2, for the Ni/Si catalyst, the Ti loadings have negative effect on the conversion and increasing the

amount of Ti can intensify the negative effect and result in slight fluctuations on the selectivity by contrasting group 1-3. On the other hand, the comparison of group 4-6 revealed that Ti loading can enhance the conversion of Co-containing catalyst and along with the increasing amount of added Ti, the conversion was greatly improved from 19.65 to 48.29%. For the NiCo-containing catalyst, adding Ti enormously increases (2.6 times) the phenol conversion to reach to a rate of 70.16% and has no negative effect on cyclohexanol selectivity (>99%), but further addition of the Ti decreases the phenol conversion rate to 58.85%. It is strange that the effect of the Ti content on catalytic activity over Ni/Si, Co/Si, and NiCo/Si were very different. We found that Co and Ti had strong metal–support interaction (proven by XPS results), leading to the formation of the active sites for phenol hydrogenation ($\text{Co}^{\delta-}-\text{O}_V-\text{Ti}^{3+}$ interface sites). In other words, when the content of Ti was low (Si-Ti ratio of 8.5:1), adding Ni had a positive effect on the metal–support interaction, and remarkably increased the catalytic activity of NiCo/Si. In contrast, when the content of Ti was high (Si-Ti ratio of 1:8.5), adding Ni decreased the interaction between Co and Ti, and led to the decline of the catalytic activity. These findings indicated that the addition of a certain amount Ti has a very positive effect on the catalytic activity of bimetal NiCo/Si catalyst. Ultimately, NiCo/Si-1.0Ti (group 8) was selected for further research.

Table 2 Catalyst screening of the hydrogenation on phenol.

Group	Catalysts	Phenol conv. (%)	Cyclohexanol sel.(%)
-------	-----------	---------------------	-------------------------

1	Ni/Si	39.36	96.87
2	Ni/Si-1.0Ti	37.03	>99
3	Ni/Si-8.5Ti	25.68	95.46
4	Co/Si	19.65	>99
5	Co/Si-1.0Ti	22.61	90.64
6	Co/Si-8.5Ti	48.29	>99
7	NiCo/Si	26.71	>99
8	NiCo/Si-1.0Ti	70.16	>99
9	NiCo/Si-8.5Ti	58.85	>99

Reaction conditions : 0.05 g phenol, 10 mL n-heptane as solvent, 0.1 g catalyst, 100 °C, 1.0 MPa H₂ and reaction time = 0.5 h.

The effect of H₂ pressure on the phenol hydrogenation performance was investigated by varying the H₂ pressure in the range of 0.5–3 MPa. As can be seen in Fig. 7a, the phenol conversion showed a trend of sharply rising and then achieved the full conversion with the increase of the H₂ pressure. It is indicated that optimum H₂ pressure is 1 MPa. The tests of reaction temperature on the conversion of phenol was carried out and the results were illustrated in Fig. 7b. It is obvious that the hydrogenation of phenol was considerably accelerated with an increase of reaction temperature from 60°C to 120°C. It was also worth noting that cyclohexanol was the only detected product in all tested reaction temperatures, revealing the excellent selectivity of NiCo/Si-1.0Ti can maintain over a wide range of temperatures.

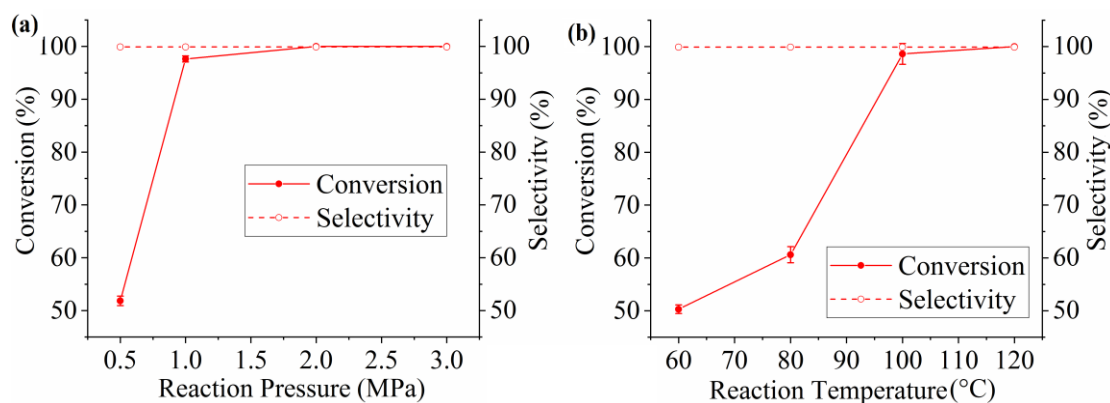


Fig. 7 Influence of H₂ pressure (a) and temperature (b) on the activity of the NiCo/Si-1.0Ti catalyst in the hydrogenation reaction of phenol. Reaction conditions: 0.05 g phenol, 10 mL n-heptane as solvent, 0.1 g catalyst, 100 °C (a), 1.0 MPa H₂ (b), and reaction time = 1 h.

The hydrogenation reaction of phenol was investigated at 100°C under 1.0 MPa using the NiCo/Si, NiCo/Si-1.0Ti, NiCo/Si-3.5Ti, NiCo/Si-6.0Ti and NiCo/Si-8.5Ti catalysts. As shown in Fig. 8a, with the increase of the reaction time, the NiCo/Si-1.0Ti catalyst showed the best performance, and achieved almost full phenol conversion (98.2%) with excellent cyclohexanol selectivity (>99%) in 1 h of reaction time. In comparison, NiCo/Si-3.5Ti, NiCo/Si-6.0Ti, NiCo/Si-8.5Ti and NiCo/Si only achieved 87.60%, 83.35%, 76.1% and 34.1%, respectively. Compared to NiCo/Si, catalytic performance of Ti-doped catalysts were improved, but that of high Ti content catalysts decreased their catalytic activity, maybe due to the decrease in porosity, as shown by the SEM and BET results. The differences in the $-\ln(C/C_0)$ versus time (t) for the NiCo/Si, NiCo/Si-1.0Ti, NiCo/Si-3.5Ti, NiCo/Si-6.0Ti and NiCo/Si-8.5Ti are shown in Fig. 8b. The reaction equation (1) is expressed as follows [61]:

$$-\ln \frac{C}{C_0} = kt \quad (1)$$

where C denotes the reaction concentration of phenol, C_0 represents the initial concentration of phenol, k is the apparent rate constant and t is the reaction time. The apparent rate constant (k) of phenol hydrogenation can be obtained from the slope of the linear fitted plot. The specific value of k for the five kinds of catalysts are listed in Table 3, and it can be seen that the k value followed the trend NiCo/Si-1.0Ti > NiCo/Si-3.5Ti > NiCo/Si-6.0Ti > NiCo/Si-8.5Ti > NiCo/Si. It reveals that doped Ti can significantly increase the hydrogenation of phenol to produce cyclohexanol, and the k value of NiCo/Si-1.0Ti was 3.6-fold higher than that of NiCo/Si, respectively. These differences suggest that NiCo/Si-1.0Ti has a considerably higher hydrogenation ability than the other four catalysts. Material balance is calculated using Eq. (2) [68]:

$$\text{Material balance} = \frac{n(\text{Phenol}) + n(\text{Cyclohexanol})}{n_0(\text{Phenol})} \quad (2)$$

where $n(\text{phenol})$ and $n(\text{cyclohexanol})$ are the amounts of phenol and cyclohexanol in hydrogenation reaction products, respectively, and $n_0(\text{phenol})$ is the amount of phenol before the hydrogenation reaction. As shown in Table 3, the material balance was $100\% \pm 1\%$. Turnover frequency (TOF) is calculated as bellow [34]:

$$\text{TOF} = \frac{n_{\text{phenol}} \times C_{\text{phenol}}}{n_{\text{metal}} \times T} \quad (3)$$

where n_{phenol} is mol of substrate; C is phenol conversion (%); n_{metal} is mol of metal atom; T is reaction time (h). In Table 3, phenol could be nearly completely converted to the cyclohexanol over the NiCo/Si-1.0Ti (conversion 98% and selectivity >99%) with a TOF value of 4.76 h^{-1} , which is approximately 2.06 times higher than that of the NiCo/Si (2.31 h^{-1}). This indicates that the interface site (e.g., $\text{Co}^{\delta-}-\text{O}_V-\text{Ti}^{3+}$) in

NiCo/Si-1.0Ti, but absent in NiCo/Si, is a key factor governing the catalytic efficiency [34]. Moreover, high Ti-loaded catalyst showed low activity for this reaction because TOF value of NiCo/Si-3.5Ti, NiCo/Si-6.0Ti and NiCo/Si-8.5Ti were slightly lower than that of NiCo/Si-1.0Ti, indicating the high amount of Ti was not very effective for creating highly active alloy-based sites.

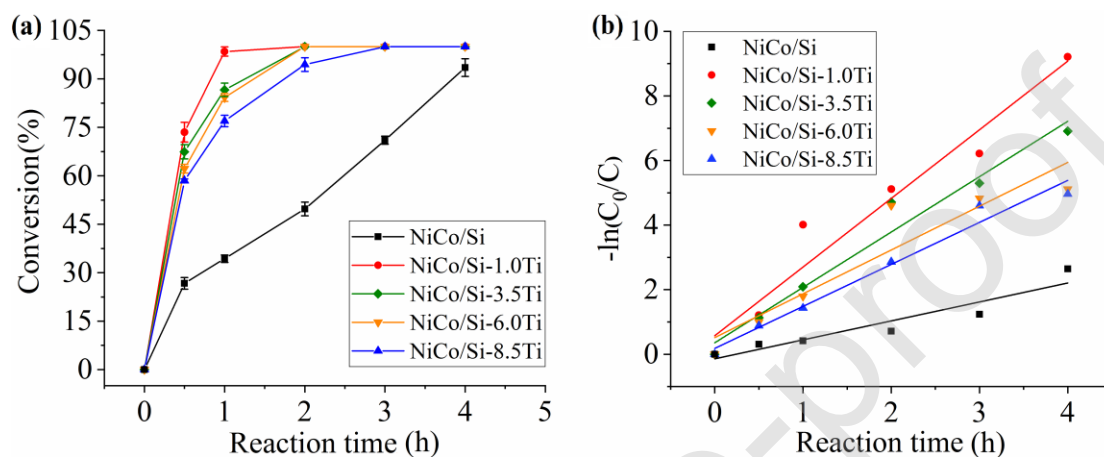


Fig. 8 Comparison of the catalytic activity of the NiCo/Si-1.0Ti, NiCo/Si-3.5Ti, NiCo/Si-6.0Ti, NiCo/Si-8.5Ti and NiCo/Si catalysts: conversion vs. reaction time of phenol (a). Plots of $-\ln(C/C_0)$ versus time (t) for the NiCo/Si-1.0Ti, NiCo/Si-3.5Ti, NiCo/Si-6.0Ti, NiCo/Si-8.5Ti and NiCo/Si (b). Reaction conditions: 0.05 g phenol, 10 mL n-heptane as solvent, 0.1 g catalyst, 100°C, and 1.0 MPa H₂.

Table 3 Catalytic performance of different catalysts in the hydrogenation reaction of phenol to cyclohexanol.^a

Entry	Catalysts	Conv. (%)	Sel.(%) (Cyclohexanol)	Rate constant k	Material balance (%)	TOF ^b (h ⁻¹)
1	NiCo/Si-1.0Ti	98.19	>99	2.126	99.50	4.76
2	NiCo/Si-3.5Ti	87.60	>99	1.714	100.45	3.48

3	NiCo/Si-6.0Ti	83.35	>99	1.357	99.33	2.93
4	NiCo/Si-8.5Ti	76.11	>99	1.301	100.34	2.24
5	NiCo/Si	34.08	>99	0.587	100.12	2.31

^a Reaction condition: 0.05 g phenol, 10 mL n-heptane as solvent, 0.1 g catalyst, 100°C, 1.0 MPa H₂ and reaction time = 1 h.

^b Mole number of phenol converted per surface metal atom per second.

A possible pathway for the selective hydrogenation of phenol to cyclohexanol was proposed in Fig. 9a. In pathway (i), the hydrogenation of phenol is a two-step reaction, i.e. phenol is firstly hydrogenated to cyclohexanone, and cyclohexanone then be further hydrogenated to cyclohexanol [69-72]. In pathway (ii), the hydrogenation reaction proceeds through a one-step process, i.e. cyclohexanol is formed directly by the one-step hydrogenation of phenol [11]. k_1 , k_2 and k are the reaction rate constants for each step in phenol hydrogenation. In this work, cyclohexanone was not detected and cyclohexanol was the only product throughout the entire reaction process even at a short reaction time (less than 10 min) and a very low phenol conversion rate (lower than 15%), and thus, $k_1 \ll k_2$. After calculated, clearly, rate constant of cyclohexanone hydrogenation to cyclohexanol ($k_2=2.581$, see Fig. S2) was almost 10-fold higher than that of phenol hydrogenation to cyclohexanol ($k=0.2611$) over NiCo/Si-1.0Ti. This indicated that cyclohexanone is too rapidly hydrogenated into cyclohexanol to be detected under this two-step reaction over NiCo/Si-1.0Ti catalyst.

A possible catalytic mechanism for the hydrogenation of phenol using the NiCo/Si-Ti catalyst is proposed in Fig. 9b. the phenol is adsorbed on the surface of NiCo/Si-1.0Ti

through the interaction between the OH and Ni-Co. The XPS analysis result of the NiCo/Si-1.0Ti catalyst indicated that the Ni²⁺ and Co²⁺ sites can potentially accept lone pairs of electrons from donating groups of Si and Ti oxide species, respectively, leading to the increase of the electron density around the Ni and Co atoms. The interaction of Ni and Co species with the π -electrons of the phenol molecules led to the formation of strong π -complex bonds between the Ni-Co and the oxygen atom of the phenol molecule, which accelerated the adsorption of phenol. Thus, the electronic interaction between Ni and Si, Co and Ti greatly influenced the adsorption capacity of phenol. Then, Ni-Co attached to the adsorbed phenol to form an electron rich intermediate. Additionally, the H₂ molecules were also dissociated into highly active H atoms under the synergic effect of the metal-support, so as to form the Co ^{δ^-} -O_v-Ti³⁺ interface sites. Afterwards, the H atoms attack the π electron of the intermediate, which leads to the hydrogenation of this intermediate. With the saturation of the benzene ring, the strength of the OH is considerably reduced, thus the interaction between the OH and Ni-Co is remarkably weakened, causing the dissociation of the final cyclohexanol product.

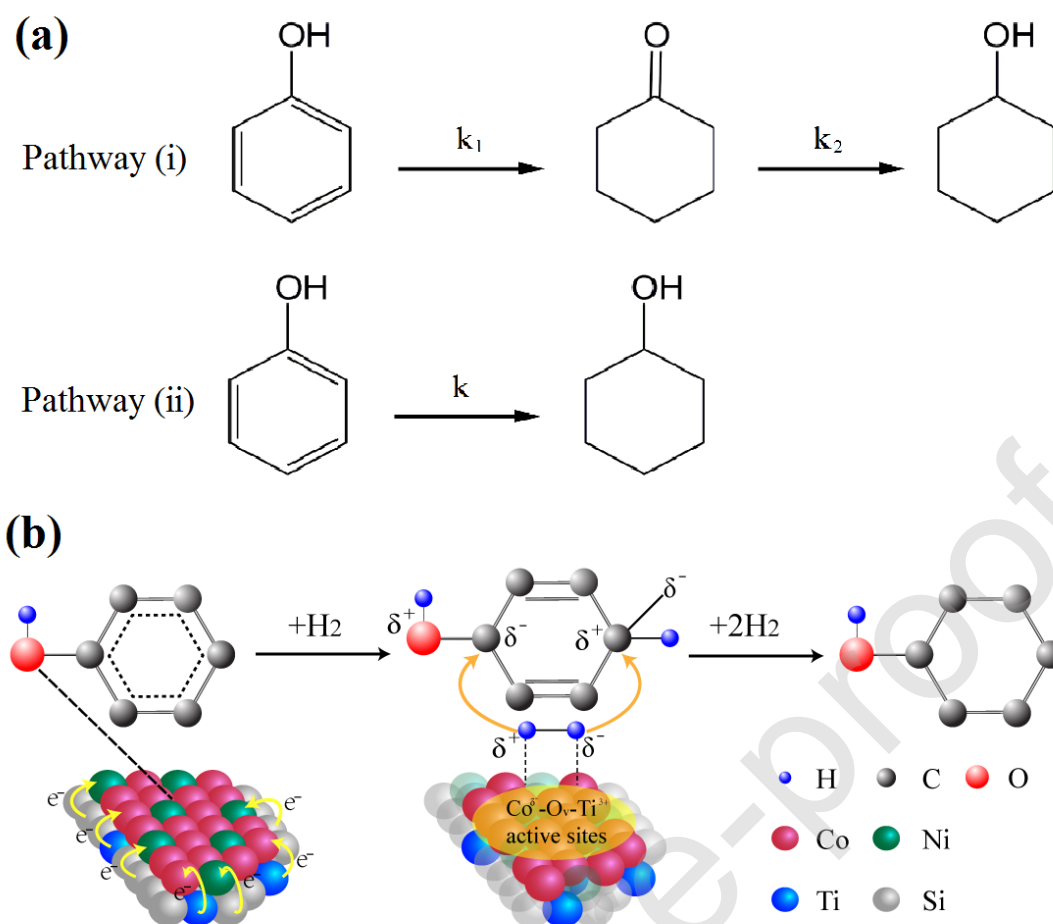


Fig. 9 Reaction pathways (a) and possible catalytic mechanism (b) of phenol

hydrogenation over the NiCo/Si-1.0Ti catalyst.

We compared our newly developed catalysts for the hydrogenation of phenol with other reported non-sulfided inexpensive metal catalysts (Table 4). The catalytic performance of NiCo/Si-1.0Ti was comparable or even superior to that of some of the previously reported inexpensive metal catalysts. However, although the reaction conditions and apparatus required for the reaction among the catalysts are different, the shorter time, lower temperature and lower pressure required with our catalysts are quite obvious under the respective optimal condition. In short, our catalysts (NiCo/Si-1.0Ti) showed high phenol conversion and cyclohexanol selectivity under

mild conditions.

Table 4 Comparison of our newly developed catalysts with other non-sulfided inexpensive metal catalysts for the hydrogenation of phenol.

Catalysts	Time (min)	Temp. (°C)	H ₂ (MPa)	Phenol con. (%)	Cyclohexanol sel. (%)
NiCo/Si-1.0Ti ^a	60	100	1	>99%	>99%
NiCo@CN [11]	720	100	0.8	>99%	>99%
NiCo@C/ZrO ₂ [27]	240	200	2	96.33	91.14
NiCo/ γ -Al ₂ O ₃ [28]	240	250	2	82.36	85
Ni/SiO ₂ [73]	240	200	1	100	100
Ni/SiO ₂ [74]	300	275	10	100	≈90
Ni/Al ₂ O ₃ [19]	240	280	4	83	--
Ni/NiO [75]	480	67	2	92	97
Ni/CeO ₂ [13]	300	275	10	100	≈90
Raney Ni [12]	120	220	2	86.75	51.9
Ni ₃ P-CePO ₄ [76]	120	150	4	≈90	≈100
CoO _x @porous carbon [9]	960	150	3	98	76.5

^a Reaction conditions: catalyst 0.1 g, phenol 50 mg, n-heptane 10 mL.

The data presented in Fig. 10a reveal that the reaction mixture became clarified very quickly when magnets were placed on the right of the bottle after 20 seconds, and this simple method was used in the recovery of the catalyst. The recovered catalysts were reused in the next run after reduction by H₂ at 300°C for 3 h. The results in Fig. 10b

show that after four consecutive runs were carried out, the conversion rate basically stayed stable at 97-100% with the selectivity remaining at 100%.

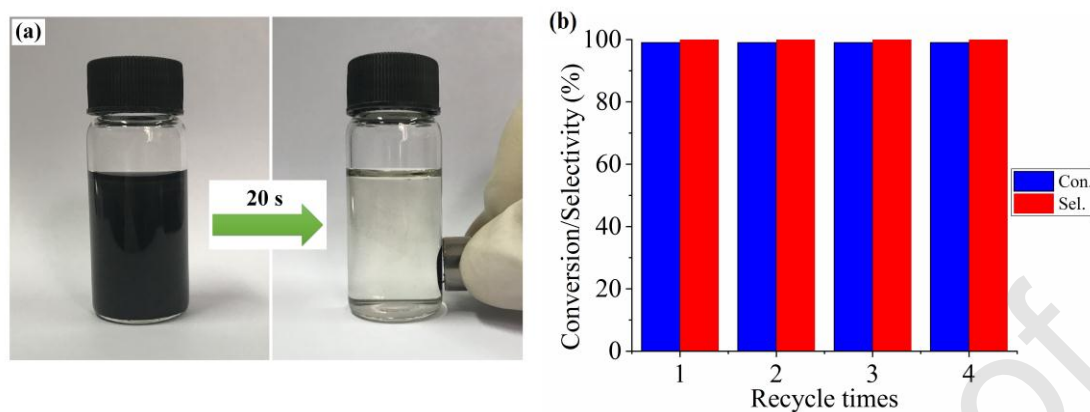
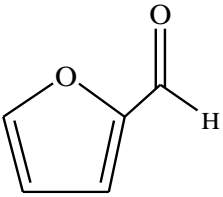
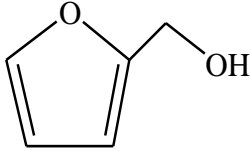
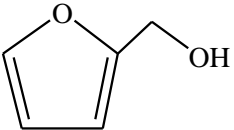
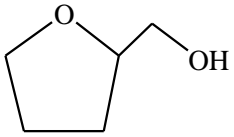
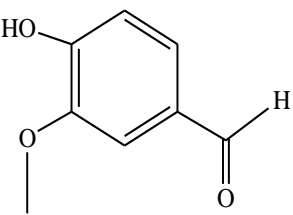
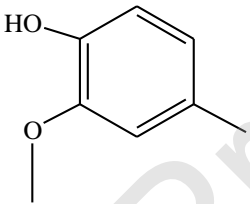


Fig. 10 Magnetic separation and recovery of the NiCo/Si-1.0Ti catalyst (a); recycling tests of the NiCo/Si-1.0Ti in the hydrogenation reaction of phenol (b).

Hydrogenation of various bio-oil model compounds (furfural, furfuryl alcohol and vanillina) over the NiCo/Si-1.0Ti catalyst was investigated and the results are shown in Table 5. Under mild conditions, furfural conversion and furfuryl alcohol selectivity were almost 100 and 80%, respectively. However, the conversion of furfuryl alcohol and the selectivity of 4-methyl-2-methoxy-phenol were inadequate in the reaction of furfuryl alcohol hydrogenation and vanillin hydrogenation, respectively. Therefore, the catalytic activity towards various reactants over NiCo/Si-1.0Ti catalyst was significantly different. We further undertook the evaluation of the catalytic activity of NiCo/Si-1.0Ti catalyst using real bio-oil as reactant.

Table 5 Hydrogenation of various bio-oil model compounds over the NiCo/Si-1.0Ti catalyst^a.

Model compounds	Product	Time/h	Conv/%	Sel./%
 furfural	 furfuryl alcohol	1	>99%	79.77
 furfuryl alcohol	 tetrahydrofurfuryl alcohol	3	40.46	84.67
 vanillin	 4-methyl-2-methoxyphenol	2	>99%	33.40

^a Reaction condition: 0.05g furfural, 10mL alcohol as solvent, 0.1g catalyst, 80°C, 1.0 MPa H₂ and reaction time = 1 h; 0.05g furfuryl alcohol, 10mL alcohol as solvent, 0.1g catalyst, 80°C, 1.0 MPa H₂ and reaction time = 3 h; 0.075g vanillin, 10mL alcohol as solvent, 0.1g catalyst, 80°C, 1.0 MPa H₂ and reaction time = 2 h.

The real bio-oil contains numerous organic constituents. According to the data shown in Fig. 11a, the raw bio-oil before the reaction was a black opaque liquid, but after the hydrogenation reaction, the bio-oil became clear and light brown. Gas chromatography analysis was used for preliminary detection of bio-oil stock solution

and bio-oil after reaction. The GC analysis results shown in Fig. 11b clearly reveal that there were significant decreases both in the component types and peak area. In addition, further analysis of the chemical composition of the bio-oil was conducted using GC-MS. The chemical composition of the raw bio-oil and the products of the hydrogenation reaction of bio-oil are shown in Table 6. In addition, GC of GC-MS and relevant retention time was showed in Fig. S3 and Table S1 (see Supporting Information), respectively.

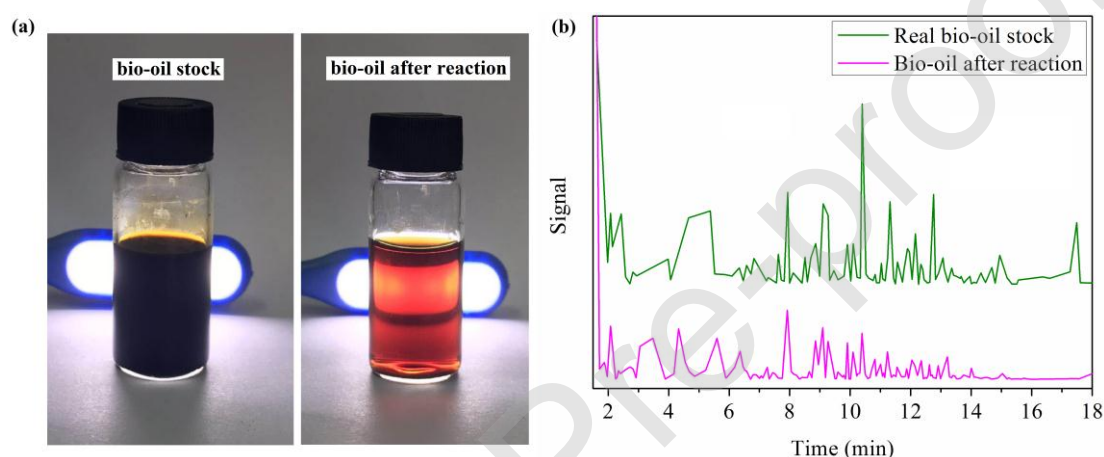


Fig. 11 Image of the mixture of bio-oil stock and bio-oil after reaction (a); GC analysis of real bio-oil test (b).

Prior to GC/MS detection, the two bio-oil samples were prepared through by diluting the bio-oil with acetone at a 1:10 ratio (v/v) and adding magnesium sulfate to remove moisture. The main identified compounds of the raw bio-oil and hydrogenated bio-oil were classified based on their functional groups as alcohols, aldehydes, ketones, phenols, esters and other types of compounds with absolute peak area and a percentage area of the individual peaks. For the raw bio-oil, phenolic compounds accounted for the largest proportion with 71.23%, among which phenol represented 33.51%. In the presence of the NiCo/Si-1.0Ti catalyst, the content of hydrogenated

bio-oil for aldehyde, ketone and ester compounds were not detected and the absolute peak area of every kind of phenolic compound was reduced, especially phenol decreased by about 55% (from 84990173 to 38131740 Ab*s). This finding is consistent with that of a previous study [77] which reported that furfural, 2-furancarboxaldehyde and 2-methoxy-2-furyl alcohol completely disappeared after hydrogenation, but part of the phenolic compounds were still found in the hydrogenated products. The removal of the aldehyde and ketone compounds may significantly improved the thermal stability of bio-oils [78, 79]. Correspondingly, the 2-butoxy-ethanol in the product was increased by 46.5% (from 4676731 to 6849491 Ab*s), probably as a result of the hydrogenation of ketones and aldehydes [80]. In addition, the resulting 3-methyl-3-hexene may be converted from partial 2-methyl-phenol. Also, 1,4-dimethoxy-2-methyl-benzene was increased almost 4.5-fold, probably through the complex reaction process of various substances. It is possible that condensation, hydrogenation and esterification reactions occur simultaneously and cause the difficulty in the analysis of the reaction pathway [78, 81]. We inferred that over the NiCo/Si-1.0Ti catalyst, the hydrogenation reaction of aldehyde, ketone and ester compounds occurred prior to that of the phenolic compound, thus phenol was still observed in the bio-oil after the reaction. Moreover, some phenolic compounds are hydrogenated to produce phenol, for example, the main hydrogenated products of eugenol is phenol, and the 4-propyl-2-methoxy-phenol in hydrogenated bio-oil is also produced by hydrogenation of eugenol [77]. The material balance was approximately 90%, and about 80% recovery yield of liquid products

was achieved. The liquid product might be on the metal reactor walls or loss of volatiles during the removal of solvent (acetone), where it would be difficult to accurately collect and quantify [79, 82].

Table 6 Major constituents of raw bio-oil and hydrogenated bio-oil analyzed by GC–MS.

Group	Chemical composition	Raw bio-oil		Reaction bio-oil	
		Absolute area/Ab*s	Percentage area of individual peaks/%	Absolute area/Ab*s	Percentage area of individual peaks/%
Phenolic compounds	4-ethyl-phenol	3728939	1.470	-	-
	hydroquinone	4034409	1.591	-	-
	eugenol	4748945	1.873	-	-
	4-ethyl-2-methoxy-phenol	7559860	2.981	2583371	2.830
	2,4-dimethyl-phenol	8212190	3.238	6652209	7.287
	2-methyl-phenol	11490468	4.531	6061791	6.640
	2,6-dimethoxy-phenol	16740349	6.601	2412559	2.643
	p-cresol	19379522	7.641	4003740	4.386
	2-methoxy-phenol	19754455	7.789	4870250	5.335
	phenol	84990173	33.512	38131740	41.772
	2-methoxy-3-methyl-p	-	-	1126217	1.234

	henol				
	3-methyl-phenol	-	-	3335793	3.654
	4-propyl-2-methoxy-p				
	henol	-	-	2910071	3.188
<hr/>					
	Aldehyd				
e	Furfural	6384525	2.517	-	-
compou					
nd					
<hr/>					
	2',4'-dihydroxyacetop				
	henone	320720	0.126	-	-
	6-(3,5-dimethyl-2-fura				
	nyl)-6-methyl-2-hepta	1192561	0.470	-	-
	none				
Ketone	VII tropolone	2345488	0.925	-	-
compou					
nd	4-(2,2,6-trimethyl-7-o				
	xabicyclo[4.1.0]hept-1	3005970	1.185	-	-
	-yl)-(E)-3-Penten-2-on				
e					
	3-methyl-1,2-cyclopen				
	tanedione	5765853	2.273	-	-
<hr/>					
Ester	2,5-pyridinedicarboxy				
compou	lic acid, dimethyl ester	13082269	5.158	-	-

nd					
	1,4-dimethoxy-2-meth	1132745	0.447	6207363	6.800
	yl-benzene				
	1-methyl-N-vanillyl-(
	+)s-2-Phenethanamin	2221777	0.876	-	-
	e				
	1,1-dioxide-Benzo[b]t	2539358	1.001	-	-
	hiophene				
Other	4-Hydroxybenzamide	3953491	1.559	-	-
types of	Bis(4-methylphenylthi				
compou	o)-methane	4128936	1.628	-	-
nds	2-butoxy-ethanol	4676731	1.844	6849491	7.503
	2-methyl-furan	4947307	1.951	-	-
	3,3-dimethoxy-6,6-di				
	methyl-cyclohexa-1,4-	4996127	1.970	-	-
	diene				
	2-methyl- 2-hexanol	12281517	4.843	-	-
	3-methyl-3-hexene	-	-	6140993	6.727

Reaction condition: 10 mL raw bio-oil, 0.5 g catalysts, 250°C, 1 MPa H₂ and reaction time = 4 h.

¹H NMR provides a additional analysis of non-chromatographable from bio-oil.

Semi-quantitative results utilizing ¹H NMR (Fig. S4) were obtained by a normalized

integration method suggested by Marjorie R. Rover et al [30], and the obtained hydrogen percentages are summarized in Table 7. The chemical shift regions evaluated by ^1H NMR were based on values from the literatures [83, 84]. The observed protons are concluded that the bio-oil after hydrogenation mainly contained ethers and aliphatic alcohols compounds (3.0-5.0 ppm) while which were not fully observed by GC-MS. Compare raw bio-oil with reaction bio-oil, protons alpha to ketones, aldehydes, phenolic alcohols, aromatics, carboxylic acids, vinyls and conjugated double bonds functional groups were decreased after hydrogenation, whereas, it showed significantly increases in the aliphatics region 0.0-1.6 ppm, ethers and aliphatic alcohols region 3.0-5.0 ppm. While a decrease in ketones and aldehydes was expected, the observed increase in the region of 3.0-5.0 ppm might be explained by the production of aliphatic alcohols. At that point, phenolic alcohols and aromatic protons was decreased, and the latter occurred in the region of 6.8-8.0 ppm creating overlap with olefinic protons, ultimately, complicating analyzes [30, 85]. The aldehydes and carboxylic acids protons in the region between 8.0-10.0 ppm were observed very less amount in the raw bio-oil (0.63%), and it was disappeared after hydrogenation. A decrease in the proton resonance of vinyls and conjugated double bonds was corresponds to saturation of carbon bonds. Furthermore, aldehyde and ketone region 2.2-3.0 ppm were not identified in reaction bio-oil from GC-MS but from ^1H NMR analysis, this demonstrated that aldehyde and/or ketone compounds were present in the reaction bio-oil. In a word, reaction bio-oil contained more aliphatic (4.49% vs. 2.81%), ethers and aliphatic alcohols protons (187.61% vs.

116.78%), and less of other proton types compared to raw bio-oil, suggesting that bio-crude oil quality can be improved by using NiCo/Si-1.0Ti catalyst.

Table 7 Proton distribution of various functionalities from raw bio-oil and reaction bio-oil.

Functional groups and structures	Chemical shifts (ppm)	%H	
		Raw bio-oil	Reaction bio-oil
Aliphatics	0.0-1.6	2.81	4.49
Aliphatics and aliphatic alcohols	1.6-2.2	4.99	4.30
Ketones and aldehydes	2.2-3.0	4.01	3.56
Ethers and aliphatic alcohols	3.0-5.0	116.78	187.61
Vinyls and phenolic alcohols	5.0-6.4	1.79	1.03
Conjugated double bonds	6.4-6.8	1.55	1.34
Aromatics	6.8-8.0	1.4	0.66
Aldehydes and carboxylic acids	8.0-10.0	0.63	0

4. Conclusion

Ti-Si-supported Ni and Co-based metal catalysts were prepared and investigated in the hydrogenation of phenol as a model compound for bio-oil. Cyclohexanol is the main product, and the conversion (98.2%) and selectivity (>99%) using the NiCo/Si-1.0Ti catalyst (Si:Ti ratio of 8.5:1) are both high under mild reaction conditions (1 MPa initial H₂ pressure and 100°C). The objective of this work was to evaluate metal-support interactions, and the optimal NiCo/Si-1.0Ti can markedly

enhance the active sites on the catalyst. According to the H₂-TPD analysis, the NiCo/Si-1.0Ti catalyst displayed the most intense H₂ desorption peak in the H₂-TPD profiles, suggesting that it had the most abundant dissociated active H, and the strongest interaction between activating centers and adsorbed H₂. XRD indicated the Co-Ti alloy only appeared in NiCo/Si-1.0Ti catalyst. The XPS analysis reveals a charge transfer from Si to Ni and Ti to Co in the metal-support interface. The strong Co-TiO_{2-x} electronic interaction can induce the formation of the Co^{δ-}-O_v-Ti³⁺ interface sites, which play an important role as active sites for the catalytic hydrogenation of phenol. In contrast to the NiCo/Si catalyst, the Ti-doped catalysts markedly improved the hydrogenation activity, and NiCo/Si-1.0Ti catalyst had the highest hydrogenation activity among the Ti-doped catalysts. The kinetics k-value and catalytic efficiency TOF-value of NiCo/Si-1.0Ti was 3.6-fold and 2.06-fold higher than that of NiCo/Si, respectively. We concluded that the catalytic hydrogenation of phenol to cyclohexanol is a two-step process and proposed a possible catalytic mechanism. For the hydrogenation of real bio-oil, no aldehyde, ketone and ester compounds were detected in the hydrogenated bio-oil by GC-MS, and from ¹H NMR analysis showed that reaction bio-oil contained more aliphatic (4.49% vs. 2.81%), ethers and aliphatic alcohols protons (187.61% vs. 116.78%), and less of other proton types compared to raw bio-oil, indicating that the NiCo/Si-1.0Ti catalyst had a good performance in reducing the unstable oxygenated compounds present in the bio-oil.

Authors' contributions

Yucheng Li: Methodology, Investigation. **Jing Liu:** Formal analysis, Writing - Original Draft. **Jing He:** Validation. **Luying Wang:** Writing - Review & Editing. **Jiandu Lei:** Supervision.

Acknowledgements

This work was financially supported by the National Natural Science Foundation of China (21808014), Beijing excellent talent training (Youth backbone individual project 2017) and Fundamental Research Funds for the Central Universities (2018ZY05).

The authors would like to thank Prof. Qiang Lu from North China Electric Power University and Dr. Chu Wang from University of Science and Technology of China for their bio-oil supply; Prof. Guoyong Song and Dr. Jialong Wen from Beijing Forestry University for his GC-MS and $^1\text{H-NMR}$ analytical support, respectively.

References

- [1] S. Gao, G. Tang, D. Hua, R. Xiong, J. Han, S. Jiang, Q. Zhang, C. Huang, Stimuli-responsive bio-based polymeric systems and their applications, *Journal of Materials Chemistry B*, 7 (2019) 709-729.
- [2] Q. Bu, H.W. Lei, A.H. Zacher, L. Wang, S.J. Ren, J. Liang, Y. Wei, Y.P. Liu, J. Tang, Q. Zhang, R. Ruan, A review of catalytic hydrodeoxygenation of lignin-derived phenols from biomass pyrolysis, *Bioresour. Technol.*, 124 (2012) 470-477.
- [3] C.C. Templis, C.J. Revelas, A.A. Papastylionou, N.G. Papayannakos, Phenol Hydrodeoxygenation over a Reduced and Sulfided NiMo/ γ -Al₂O₃ Catalyst, *Industrial & Engineering Chemistry Research*, 58 (2019) 6278-6287.
- [4] Q.Q. Guan, B. Wang, X.S. Chai, J. Liu, J.J. Gu, P. Ning, Comparison of Pd-UiO-66 and Pd-UiO-66-NH₂ catalysts performance for phenol hydrogenation in aqueous medium, *Fuel*, 205 (2017) 130-141.
- [5] Q. Zhang, H. Li, P. Gao, L. Wang, PVP-NiB amorphous catalyst for selective hydrogenation of phenol and its derivatives, *Chinese Journal of Catalysis*, 35 (2014) 1793-1799.
- [6] D. Li, Z. Wu, D. Zhou, Y. Xia, X. Lu, H. He, Q. Xia, One-step synthesis of hybrid zeolite with exceptional hydrophobicity to accelerate the interfacial reaction at low temperature, *Microporous and Mesoporous Materials*, 280 (2019) 195-202.
- [7] E. Díaz, A.F. Mohedano, L. Calvo, M.A. Gilarranz, J.A. Casas, J.J. Rodríguez, Hydrogenation of phenol in aqueous phase with palladium on activated carbon catalysts, *Chemical Engineering Journal*, 131 (2007) 65-71.
- [8] J. Long, S. Shu, Q. Wu, Z. Yuan, T. Wang, Y. Xu, X. Zhang, Q. Zhang, L. Ma, Selective cyclohexanol production from the renewable lignin derived phenolic chemicals catalyzed by Ni/MgO, *Energy Conversion and Management*, 105 (2015) 570-577.
- [9] Z. Wei, Y. Li, J. Wang, H. Li, Y. Wang, Chemoselective hydrogenation of phenol to cyclohexanol using heterogenized cobalt oxide catalysts, *Chinese Chemical Letters*, 29 (2018) 815-818.
- [10] J. He, X.H. Lu, Y. Shen, R. Jing, R.F. Nie, D. Zhou, Q.H. Xia, Highly selective hydrogenation of phenol to cyclohexanol over nano silica supported Ni catalysts in aqueous medium, *Molecular Catalysis*, 440 (2017) 87-95.
- [11] A. Li, K. Shen, J. Chen, Z. Li, Y. Li, Highly selective hydrogenation of phenol to cyclohexanol over MOF-derived non-noble Co-Ni@NC catalysts, *Chemical Engineering Science*, 166 (2017) 66-76.
- [12] R.D.D. Putra, H.L. Trajano, S. Liu, H. Lee, K. Smith, C.S. Kim, In-situ glycerol aqueous phase reforming and phenol hydrogenation over Raney Ni, *Chemical Engineering Journal*, 350 (2018) 181-191.
- [13] P.M. Mortensen, J.-D. Grunwaldt, P.A. Jensen, A.D. Jensen, Screening of Catalysts for Hydrodeoxygenation of Phenol as a Model Compound for Bio-oil, *ACS Catalysis*, 3 (2013) 1774-1785.

- [14] C.A. Teles, R.C. Rabelo-Neto, G. Jacobs, B.H. Davis, D.E. Resasco, F.B. Noronha, Hydrodeoxygenation of Phenol over Zirconia-Supported Catalysts: The Effect of Metal Type on Reaction Mechanism and Catalyst Deactivation, *Chemcatchem*, 9 (2017) 2850-2863.
- [15] D. Liu, G.F. Li, F.F. Yang, H. Wang, J.Y. Han, X.L. Zhu, Q.F. Ge, Competition and Cooperation of Hydrogenation and Deoxygenation Reactions during Hydrodeoxygenation of Phenol on Pt(111), *Journal of Physical Chemistry C*, 121 (2017) 12249-12260.
- [16] H. Chen, Y.L. He, L.D. Pfefferle, W.H. Pu, Y.L. Wu, S.T. Qi, Phenol Catalytic Hydrogenation over Palladium Nanoparticles Supported on Metal-Organic Frameworks in the Aqueous Phase, *Chemcatchem*, 10 (2018) 2558-2570.
- [17] V. Vinokurov, A. Glotov, Y. Chudakov, A. Stavitskaya, E. Ivanov, P. Gushchin, A. Zolotukhina, A. Maximov, E. Karakhanov, Y. Lvov, Core/Shell Ruthenium Halloysite Nanocatalysts for Hydrogenation of Phenol, *Industrial & Engineering Chemistry Research*, 56 (2017) 14043-14052.
- [18] G.Y. Xu, J.H. Guo, Y.C. Qu, Y. Zhang, Y. Fu, Q.X. Guo, Selective hydrodeoxygenation of lignin-derived phenols to alkyl cyclohexanols over a Ru-solid base bifunctional catalyst, *Green Chemistry*, 18 (2016) 5510-5517.
- [19] Z. Wang, Y. Zeng, W. Lin, W. Song, In-situ hydrodeoxygenation of phenol by supported Ni catalyst – explanation for catalyst performance, *International Journal of Hydrogen Energy*, 42 (2017) 21040-21047.
- [20] Y.H. Li, X. Yang, L.H. Zhu, H. Zhang, B.H. Chen, Hydrodeoxygenation of phenol as a bio-oil model compound over intimate contact noble metal-Ni₂P/SiO₂ catalysts, *Rsc Advances*, 5 (2015) 80388-80396.
- [21] H.W. Zhang, A. Han, K. Okumura, L.X. Zhong, S.Z. Li, S. Jaenicke, G.K. Chuah, Selective hydrogenation of phenol to cyclohexanone by SiO₂-supported rhodium nanoparticles under mild conditions, *Journal of Catalysis*, 364 (2018) 354-365.
- [22] K.A. Resende, C.A. Teles, G. Jacobs, B.H. Davis, D.C. Cronauer, A.J. Kropf, C.L. Marshall, C.E. Hori, F.B. Noronha, Hydrodeoxygenation of phenol over zirconia supported Pd bimetallic catalysts. The effect of second metal on catalyst performance, *Applied Catalysis B-Environmental*, 232 (2018) 213-231.
- [23] Q. Han, M.U. Rehman, J.H. Wang, A. Rykov, O.Y. Gutierrez, Y.J. Zhao, S.P. Wang, X.B. Ma, J.A. Lercher, The synergistic effect between Ni sites and Ni-Fe alloy sites on hydrodeoxygenation of lignin-derived phenols, *Applied Catalysis B-Environmental*, 253 (2019) 348-358.
- [24] K.A. Resende, A.H. Braga, F.B. Noronha, C.E. Hori, Hydrodeoxygenation of phenol over Ni/Ce_{1-x}Nb_xO₂ catalysts, *Applied Catalysis B-Environmental*, 245 (2019) 100-113.
- [25] J.L. Tao, L.J. Liu, P.H. Zhu, K. Zhai, Q. Ma, D.N. Zhang, J. Ma, Y.P. Zhai, Y.G. Liu, R.Q. Zhang, Dual-template synthesis of cage-like Ni-based catalyst for hydrotreatment of bio-oil, *Journal of Porous Materials*, 26 (2019) 819-828.
- [26] E. Kordouli, B. Pawelec, C. Kordulis, A. Lycourghiotis, J.L.G. Fierro, Hydrodeoxygenation of phenol on bifunctional Ni-based catalysts: Effects of Mo promotion and support, *Applied Catalysis B-Environmental*, 238 (2018) 147-160.

- [27] L. He, Z. Niu, R. Miao, Q. Chen, Q. Guan, P. Ning, Selective hydrogenation of phenol by the porous Carbon/ZrO₂ supported NiCo nanoparticles in subcritical water medium, *Journal of Cleaner Production*, 215 (2019) 375-381.
- [28] Y. Shi, S. Chen, L. He, P. Ning, Q. Guan, Selective Conversion of Phenol in a Subcritical Water Medium Using γ -Al₂O₃ Supported Ni–Co Bimetallic Catalyst, *Catalysts*, 9 (2019) 212.
- [29] C. Wang, Z. Luo, R. Diao, X. Zhu, Study on the effect of condensing temperature of walnut shells pyrolysis vapors on the composition and properties of bio-oil, *Bioresource Technology*, 285 (2019) 121370.
- [30] M.R. Rover, P.H. Hall, P.A. Johnston, R.G. Smith, R.C. Brown, Stabilization of bio-oils using low temperature, low pressure hydrogenation, *Fuel*, 153 (2015) 224-230.
- [31] J. Ren, H. Li, Y. Jin, J. Zhu, S. Liu, J. Lin, Z. Li, Silica/titania composite-supported Ni catalysts for CO methanation: effects of Ti species on the activity, anti-sintering, and anti-coking properties, *Applied Catalysis B: Environmental*, 201 (2017) 561-572.
- [32] X. Song, Q. Guan, Z. Cheng, W. Li, Eco-friendly controllable synthesis of highly dispersed ZIF-8 embedded in porous Al₂O₃ and its hydrogenation properties after encapsulating Pt nanoparticles, *Applied Catalysis B: Environmental*, 227 (2018) 13-23.
- [33] B. Xue, K. Li, S. Gu, J. Lu, Zeolitic imidazolate frameworks (ZIFs)-derived Ni_xCo_{3-x}O₄/CNTs nanocomposites with enhanced electrochemical performance for supercapacitor, *Journal of Colloid and Interface Science*, 530 (2018) 233-242.
- [34] M. Xu, S. He, H. Chen, G. Cui, L. Zheng, B. Wang, M. Wei, TiO_{2-x}-Modified Ni Nanocatalyst with Tunable Metal–Support Interaction for Water–Gas Shift Reaction, *ACS Catalysis*, 7 (2017) 7600-7609.
- [35] P.P. Upare, M.-G. Jeong, Y.K. Hwang, D.H. Kim, Y.D. Kim, D.W. Hwang, U.H. Lee, J.-S. Chang, Nickel-promoted copper–silica nanocomposite catalysts for hydrogenation of levulinic acid to lactones using formic acid as a hydrogen feeder, *Applied Catalysis A: General*, 491 (2015) 127-135.
- [36] Z. Zhang, Z. Pei, H. Chen, K. Chen, Z. Hou, X. Lu, P. Ouyang, J. Fu, Catalytic in-Situ Hydrogenation of Furfural over Bimetallic Cu–Ni Alloy Catalysts in Isopropanol, *Industrial & Engineering Chemistry Research*, 57 (2018) 4225-4230.
- [37] P. Zhou, C. Yu, L. Jiang, K. Lv, Z. Zhang, One-pot reductive amination of carbonyl compounds with nitro compounds with CO/H₂O as the hydrogen donor over non-noble cobalt catalyst, *Journal of Catalysis*, 352 (2017) 264-273.
- [38] A. Nadar, A.M. Banerjee, M.R. Pai, R.V. Pai, S.S. Meena, R. Tewari, A.K. Tripathi, Catalytic properties of dispersed iron oxides Fe₂O₃/MO₂ (M = Zr, Ce, Ti and Si) for sulfuric acid decomposition reaction: Role of support, *International Journal of Hydrogen Energy*, 43 (2018) 37-52.
- [39] H. Wang, X. Li, X. Lan, T. Wang, Supported Ultrafine NiCo Bimetallic Alloy Nanoparticles Derived from Bimetal–Organic Frameworks: A Highly Active Catalyst for Furfuryl Alcohol Hydrogenation, *ACS Catalysis*, 8 (2018) 2121-2128.
- [40] M. He, J. Yao, Q. Liu, K. Wang, F. Chen, H. Wang, Facile synthesis of zeolitic

- imidazolate framework-8 from a concentrated aqueous solution, *Microporous and Mesoporous Materials*, 184 (2014) 55-60.
- [41] A. Tanimu, S.A. Ganiyu, S. Adamu, K. Alhooshani, Synthesis, application and kinetic modeling of CeO_x-Si-CoMo catalysts for the hydrodesulfurization of dibenzothiophene, *Reaction Chemistry & Engineering*, 4 (2019) 724-737.
- [42] X. Yu, Y. Li, S. Xin, P. Yuan, W. Yuan, Partial Hydrogenation of Benzene to Cyclohexene on Ru@XO₂ (X = Ti, Zr, or Si), *Industrial & Engineering Chemistry Research*, 57 (2018) 1961-1967.
- [43] Z. Zhang, P. Zhang, K. Guo, G. Liang, H. Chen, B. Liu, J. Kong, Facile synthesis of fluorescent Au@SiO₂ nanocomposites for application in cellular imaging, *Talanta*, 85 (2011) 2695-2699.
- [44] M.A.F.e. Santos, I.P. Lôbo, R.S.d. Cruz, Synthesis and characterization of novel ZrO₂-SiO₂ mixed oxides, *Materials Research*, 17 (2014) 700-707.
- [45] X. Qiao, L. Niu, H. Zhang, X. Wen, Y. Cao, G. Bai, Controllable fabrication of a novel porous Ni-alginate hybrid material for hydrogenation, *Applied Catalysis B: Environmental*, 218 (2017) 721-730.
- [46] J. Ren, Z. Li, S. Liu, Y. Xing, K. Xie, Silica-Titania mixed Oxides: Si-O-Ti Connectivity, Coordination of Titanium, and Surface Acidic Properties, *Catalysis Letters*, 124 (2008) 185-194.
- [47] H. Duan, Z. Wang, L. Cui, B. Lin, Y. Zhou, Stability Investigation of a Supported TiO₂-Pd Bifunctional Catalyst over the One-Pot Liquid-Phase Synthesis of Methyl Isobutyl Ketone from Acetone and H₂, *Industrial & Engineering Chemistry Research*, 57 (2018) 12358-12366.
- [48] A. Hilonga, J.-K. Kim, P.B. Sarawade, H.T. Kim, Rapid synthesis of homogeneous titania-silica composite with high-BET surface area, *Powder Technology*, 199 (2010) 284-288.
- [49] J. Shim, C. Venkata Reddy, G.V.S.S. Sarma, P. Narayana Murthy, R.V.S.S.N. Ravikumar, Effect of Co²⁺ and Ni²⁺-doped zinc borate nano crystalline powders by co-precipitation method, *Spectrochimica Acta Part A: Molecular and Biomolecular Spectroscopy*, 142 (2015) 279-285.
- [50] F. Yang, D. Liu, H. Wang, X. Liu, J. Han, Q. Ge, X. Zhu, Geometric and electronic effects of bimetallic Ni-Re catalysts for selective deoxygenation of m-cresol to toluene, *Journal of Catalysis*, 349 (2017) 84-97.
- [51] L. Zhang, Z. Xing, H. Zhang, Z. Li, X. Wu, X. Zhang, Y. Zhang, W. Zhou, High thermostable ordered mesoporous SiO₂-TiO₂ coated circulating-bed biofilm reactor for unpredictable photocatalytic and biocatalytic performance, *Applied Catalysis B: Environmental*, 180 (2016) 521-529.
- [52] M. Lu, Y. Sun, P. Zhang, J. Zhu, M. Li, Y. Shan, J. Shen, C. Song, Hydrodeoxygenation of Guaiacol Catalyzed by High-Loading Ni Catalysts Supported on SiO₂-TiO₂ Binary Oxides, *Industrial & Engineering Chemistry Research*, 58 (2019) 1513-1524.
- [53] W. Sun, Y. Sun, K.J. Shah, H. Zheng, B. Ma, Electrochemical degradation of oxytetracycline by Ti-Sn-Sb/ γ -Al₂O₃ three-dimensional electrodes, *Journal of Environmental Management*, 241 (2019) 22-31.

- [54] T. Dippong, E.A. Levei, O. Cadar, F. Goga, D. Toloman, G. Borodi, Thermal behavior of Ni, Co and Fe succinates embedded in silica matrix, *Journal of Thermal Analysis and Calorimetry*, 136 (2019) 1587-1596.
- [55] L. Song, C. Xue, H. Xia, S. Qiu, L. Sun, H. Chen, Effects of Alkali Metal (Li, Na, and K) Incorporation in NH₂-MIL125(Ti) on the Performance of CO₂ Adsorption, *Materials*, 12 (2019) 844.
- [56] S. Hu, M. Liu, K. Li, Y. Zuo, A. Zhang, C. Song, G. Zhang, X. Guo, Solvothermal synthesis of NH₂-MIL-125(Ti) from circular plate to octahedron, *CrystEngComm*, 16 (2014) 9645-9650.
- [57] S.A. Ganiyu, S.A. Ali, K. Alhooshani, Simultaneous HDS of DBT and 4, 6-DMDBT over single-pot Ti-SBA-15-NiMo catalysts: influence of Si/Ti ratio on the structural properties, dispersion and catalytic activity, *RSC Advances*, 7 (2017) 21943-21952.
- [58] R. Nie, H. Yang, H. Zhang, X. Yu, X. Lu, D. Zhou, Q. Xia, Mild-temperature hydrodeoxygenation of vanillin over porous nitrogen-doped carbon black supported nickel nanoparticles, *Green Chemistry*, 19 (2017) 3126-3134.
- [59] M. Sun, J. Xia, H. Wang, X. Liu, Q. Xia, Y. Wang, An efficient Ni₃Zr₂O₇ catalyst for hydrogenation of bio-derived methyl levulinate to γ -valerolactone in water under low hydrogen pressure, *Applied Catalysis B: Environmental*, 227 (2018) 488-498.
- [60] K. Tao, Y. Gong, J. Lin, Low-temperature synthesis of NiS/MoS₂/C nanowires/nanoflakes as electrocatalyst for hydrogen evolution reaction in alkaline medium via calcining/sulfurizing metal-organic frameworks, *Electrochimica Acta*, 274 (2018) 74-83.
- [61] K. Kalantari, M. Kalbasi, M. Sohrabi, S.J. Royaei, Synthesis and characterization of N-doped TiO₂ nanoparticles and their application in photocatalytic oxidation of dibenzothiophene under visible light, *Ceramics International*, 42 (2016) 14834-14842.
- [62] K. Kalantari, M. Kalbasi, M. Sohrabi, S.J. Royaei, Enhancing the photocatalytic oxidation of dibenzothiophene using visible light responsive Fe and N co-doped TiO₂ nanoparticles, *Ceramics International*, 43 (2017) 973-981.
- [63] X. Sun, A.H.M.S. Hussain, M. Chi, X. Cheng, B.J. Tatarchuk, Persistent adsorptive desulfurization enhancement of TiO₂ after one-time ex-situ UV-treatment, *Fuel*, 193 (2017) 95-100.
- [64] M. Xu, S. Yao, D. Rao, Y. Niu, N. Liu, M. Peng, P. Zhai, Y. Man, L. Zheng, B. Wang, B. Zhang, D. Ma, M. Wei, Insights into Interfacial Synergistic Catalysis over Ni@TiO_{2-x} Catalyst toward Water-Gas Shift Reaction, *Journal of the American Chemical Society*, 140 (2018) 11241-11251.
- [65] Y. Li, Y. Fan, H. Yang, B. Xu, L. Feng, M. Yang, Y. Chen, Strong metal-support interaction and catalytic properties of anatase and rutile supported palladium catalyst Pd/TiO₂, *Chemical Physics Letters*, 372 (2003) 160-165.
- [66] S. Riyapan, Y. Boonyongmaneerat, O. Mekasuwandumrong, P. Praserthdam, J. Panpranot, Effect of surface Ti³⁺ on the sol-gel derived TiO₂ in the selective acetylene hydrogenation on Pd/TiO₂ catalysts, *Catalysis Today*, 245 (2015) 134-138.
- [67] O.U. Valdés-Martínez, V.A. Suárez-Toriello, J.A.d.l. Reyes, B. Pawelec, J.L.G.

- Fierro, Support effect and metals interactions for NiRu/Al₂O₃, TiO₂ and ZrO₂ catalysts in the hydrodeoxygenation of phenol, *Catalysis Today*, 296 (2017) 219-227.
- [68] A. Kinoshita, K. Nakanishi, R. Yagi, A. Tanaka, K. Hashimoto, H. Kominami, Hydrogen-free ring hydrogenation of phenol to cyclohexanol over a rhodium-loaded titanium(IV) oxide photocatalyst, *Applied Catalysis A: General*, 578 (2019) 83-88.
- [69] G. Li, J. Han, H. Wang, X. Zhu, Q. Ge, Role of Dissociation of Phenol in Its Selective Hydrogenation on Pt(111) and Pd(111), *ACS Catalysis*, 5 (2015) 2009-2016.
- [70] H. Liu, T. Jiang, B. Han, S. Liang, Y. Zhou, Selective Phenol Hydrogenation to Cyclohexanone Over a Dual Supported Pd–Lewis Acid Catalyst, *Science*, 326 (2009) 1250.
- [71] N. Mahata, V. Vishwanathan, Influence of Palladium Precursors on Structural Properties and Phenol Hydrogenation Characteristics of Supported Palladium Catalysts, *Journal of Catalysis*, 196 (2000) 262-270.
- [72] Y. Pérez, M. Fajardo, A. Corma, Highly selective palladium supported catalyst for hydrogenation of phenol in aqueous phase, *Catalysis Communications*, 12 (2011) 1071-1074.
- [73] J. He, X.H. Lu, Y. Shen, R. Jing, R.F. Nie, D. Zhou, Q.H. Xia, Highly selective hydrogenation of phenol to cyclohexanol over nano silica supported Ni catalysts in aqueous medium, *Molecular Catalysis*, 440 (2017) 87-95.
- [74] P.M. Mortensen, J.-D. Grunwaldt, P.A. Jensen, A.D. Jensen, Influence on nickel particle size on the hydrodeoxygenation of phenol over Ni/SiO₂, *Catalysis Today*, 259 (2016) 277-284.
- [75] H. Singh, N. Iyengar, P. Rajput, A.K. Sinha, Magnetically recoverable support-free mesoporous Ni/NiO catalyst for conversion of oxygenates to fuels and chemicals, *Materials Research Bulletin*, 112 (2019) 363-375.
- [76] Z. Yu, Y. Wang, S. Liu, Y. Yao, Z. Sun, X. Li, Y. Liu, W. Wang, A. Wang, D.M. Camaioni, J.A. Lercher, Aqueous Phase Hydrodeoxygenation of Phenol over Ni₃P-CePO₄ Catalysts, *Industrial & Engineering Chemistry Research*, 57 (2018) 10216-10225.
- [77] J. Feng, Z. Yang, C. Hse, Q. Su, K. Wang, J. Jiang, J. Xu, In situ catalytic hydrogenation of model compounds and biomass-derived phenolic compounds for bio-oil upgrading, *Renewable energy*, 105 (2017) 140-148.
- [78] H. Wang, S. Lee, M.V. Olarte, A.H. Zacher, Bio-oil Stabilization by Hydrogenation over Reduced Metal Catalysts at Low Temperatures, *ACS Sustainable Chemistry & Engineering*, 4 (2016) 5533-5545.
- [79] H.P.R. Kannapu, C.A. Mullen, Y. Elkasabi, A.A. Boateng, Catalytic transfer hydrogenation for stabilization of bio-oil oxygenates: Reduction of p-cresol and furfural over bimetallic Ni–Cu catalysts using isopropanol, *Fuel processing technology*, 137 (2015) 220-228.
- [80] H. Bergem, R. Xu, R.C. Brown, G.W. Huber, Low temperature aqueous phase hydrogenation of the light oxygenate fraction of bio-oil over supported ruthenium catalysts, *Green Chemistry*, 19 (2017) 3252-3262.
- [81] Y. Xu, J. Long, Q. Liu, Y. Li, C. Wang, Q. Zhang, W. Lv, X. Zhang, S. Qiu, T. Wang, In situ hydrogenation of model compounds and raw bio-oil over Raney Ni

- catalyst, *Energy conversion and management*, 89 (2015) 188-196.
- [82] Q. Guan, Y. Zeng, J. Shen, X.-S. Chai, J. Gu, R. Miao, B. Li, P. Ning, Selective hydrogenation of phenol by phosphotungstic acid modified Pd/Ce-AlO_x catalyst in high-temperature water system, *Chemical Engineering Journal*, 299 (2016) 63-73.
- [83] L. Yan, Y. Wang, J. Li, Y. Zhang, L. Ma, F. Fu, B. Chen, H. Liu, Hydrothermal liquefaction of *Ulva prolifera* macroalgae and the influence of base catalysts on products, *Bioresource Technology*, 292 (2019) 121286.
- [84] Y. Ding, C. Zhao, Z. Liu, Catalytic hydrothermal liquefaction of rice straw for production of monomers phenol over metal supported mesoporous catalyst, *Bioresource Technology*, 294 (2019) 122097.
- [85] L. Ingram, D. Mohan, M. Bricka, P. Steele, D. Strobel, D. Crocker, B. Mitchell, J. Mohammad, K. Cantrell, C.U. Pittman, Pyrolysis of Wood and Bark in an Auger Reactor: Physical Properties and Chemical Analysis of the Produced Bio-oils, *Energy & Fuels*, 22 (2008) 614-625.